Convective Generation of Gravity Waves in Venus's Atmosphere: Gravity Wave Spectrum and Momentum Transport*

STEPHEN S. LEROY AND ANDREW P. INGERSOLL

Division of Geological and Planetary Sciences, California Institute of Technology, Pasadena, California

(Manuscript received 31 October 1994, in final form 7 April 1995)

ABSTRACT

The emission of internal gravity waves from a layer of dry convection embedded within a stable atmosphere with static stability and zonal winds varying in height is calculated. This theory is applied to Venus to investigate whether these waves can help support the westward maximum of angular momentum of Venus's middle atmosphere. The emission mechanism is similar to that suggested for driving the gravity modes of the Sun and relates the amplitude and spectrum of the waves to the amplitude and spectrum of the convection. Waves are damped by several mechanisms: wavebreaking in the stable atmosphere, critical layer absorption, reabsorption by the convection, and wave radiation to space. The authors use plane parallel geometry without rotation and assume sinusoidal wave fluctuations in the horizontal dimensions. The vertical dependence is determined using the WKBJ approximation.

It is found that convectively generated gravity waves do not exert an acceleration where the westward winds are greatest. Instead, they deposit westward momentum in a 1-km thick layer just above the convection. Other waves deposit eastward momentum far above the westward wind maximum where decelerations can exceed 20 m s^{-1} day^{-1}, comparable to deceleration amplitudes in Earth's mesosphere. Although the momentum fluxes by gravity waves are substantial, the vertical profile of acceleration does not match what is required for supporting Venus's atmospheric superrotation.

1. Introduction

In this paper we present a theory of internal gravity wave generation by, and propagation from, an infinite horizontal convecting layer embedded in an otherwise stable atmosphere with shear. Our intent is to investigate how waves generated by this mechanism may support the rapid rotation of Venus's atmosphere. In the investigation we theoretically calculate a spectrum of waves emitted from dry convection. In an accompanying paper we test our theory against observations by using our gravity wave spectra in simulating radio scintillation data obtained by the Pioneer Venus mission. We then compare our simulations to the Pioneer Venus data.

Many theories have been published over the past two dozen years concerning Venus's atmospheric superrotation (see Schubert 1983). Any theory of the superrotation must explain how Venus's atmosphere can maintain a local maximum in the westward angular momentum per unit mass at an altitude of about 70 km above the equator. Such a local maximum cannot persist in the presence of friction in a zonally symmetric Hadley circulation [no eddies to redistribute angular momentum over large scales; Hide (1969, 1970)]. Therefore, some nonzonally symmetric disturbance, such as an eddy or a wave, must be responsible for creating the maximum in the angular momentum per unit mass at the equatorial cloud tops (e.g., Gierasch 1975).

Hou and Goody (1985) have performed a diagnostic analysis in which they have calculated how waves and eddies redistribute angular momentum in Venus's atmosphere given the heating rates of Young and Pollack (1977). Their results show patterns of Eliassen–Palm flux divergences required to sustain different models of the mean flow. This diagnostic study is helpful in understanding the superrotation but, by its nature, it cannot determine which waves and eddies are responsible for driving the superrotation. Nevertheless, it is suggested by these authors that a vertical redistribution of zonal momentum is likely in the cloud layer between 45- and 70-km altitude in order to support the strong shear in that region. Hou and Farrell (1987) have postulated that small-scale gravity waves can pro-

* Division of Geological and Planetary Sciences of the California Institute of Technology Contribution Number 5458.

Corresponding author address: Dr. Stephen S. Leroy, Earth and Space Sciences Division, 183-355 Jet Propulsion Laboratory, California Institute of Technology, 4800 Oak Grove Dr., Pasadena, CA 91109.
E-mail: Stephen.Leroy@jpl.nasa.gov

vide the necessary momentum flux divergence in this region, but no theoretical or observational foundation exists to validate or invalidate this postulate.

We investigate the hypothesis that internal gravity waves at cloud levels in Venus's atmosphere can support the superrotation. Our focus is on small-scale waves generated by turbulent convection within the Venus clouds. These waves can exert a westward impulse in a limited region above their source and/or an eastward impulse in a limited region below their source on a global scale. The impulses arise when the vertically propagating waves are dissipated and they lose some of their associated momentum flux. Possible dissipation mechanisms include radiative and viscous decay, but the mechanisms of prime importance in this theory are critical layer absorption and wavebreaking.

A critical layer absorption mechanism for vertically propagating internal gravity waves provides an acceleration profile with the right sign for sustaining a strong shear flow. Intuitively, convection located at an altitude z_s, will generate gravity waves that propagate westward and eastward with respect to the mean flow at the altitude of the convection. Waves that propagate upward from the convection with horizontal phase speeds of $\bar{u}(z_s) - \Delta c_x$ [where $\bar{u}(z_s)$ is large and negative and Δc_x is small and positive] are critically absorbed by the mean flow because $\bar{u}(z)$ becomes increasingly negative with height in Venus's middle atmosphere. Since such a wave moves westward with respect to the flow at the source altitude, it carries westward momentum vertically. Therefore, it will deposit westward momentum where it is critically absorbed (Booker and Bretherton 1967). To conserve momentum, an eastward impulse is exerted on the mean flow at z_s. Waves that propagate upward with horizontal phase speeds of $\bar{u}(z_s) + \Delta c_x$ are not critically absorbed within the wind shear immediately above the source but are either reflected back down to their source or are dissipated at great heights by some other mechanism such as radiative damping or friction. Thus, critical layer absorption acts to maintain the shear in the mean flow near the altitude of the convection.

Observational evidence suggests the presence of convection and gravity wave activity in Venus's middle atmosphere. The four Pioneer Venus descent probes detected nearly adiabatic temperature gradients in a layer between 49- and 54-km altitude (Seiff et al. 1980), evidence for convective activity in this layer. Convective activity in this layer was sensed in situ by the VEGA balloons. These balloons floated at 54-km altitude in Venus's atmosphere and traversed a horizontal distance of over 11 000 km within about 10° of the equator (Sagdeev et al. 1986a). Each balloon experienced vertical wind fluctuations with an amplitude of about 1 m s^{-1} and periodically saw downdrafts as large as 3.5 m s^{-1} (Sagdeev et al. 1986b). Of the wind and temperature variances encountered, most were caused by convective activity, but about 15% has been identified as gravity wave activity (Ingersoll et al. 1987). Woo and Armstrong (1980) have performed statistical analyses on short timescale fluctuations seen in radio occultation data taken during the first season of the Pioneer Venus mission. The fluctuations were seen only in the stable portions of the atmosphere at 45- and 60-km altitude. The phase fluctuations and the intensity of the radio signal are caused by density variations in the planet's atmosphere, which may be caused by gravity waves.

We first use an analytic theory for the generation of gravity waves by convection developed for helioseismology (Goldreich and Kumar 1990; GK hereafter). This theory assumes that the mean wind and static stability are independent of height in the stable portion of the atmosphere. The region of convection is assumed adiabatic. Most of the waves have horizontal phase speeds on the order of the speed of convective motions. Since these are expected to be about 3–5 m s^{-1} in the Venus middle atmospheric convection, it might seem unlikely that convectively generated waves could drive the zonal wind maximum, where the westward winds are 60 m s^{-1} greater than at the convection. It is possible, though, that waves that propagate obliquely to the zonal winds can transport zonal momentum up to the zonal wind maximum because they have much higher phase speeds when projected onto the zonal axis.

We then track a three-dimensional spectrum of waves (in frequency and zonal and meridional wavenumber) as they propagate vertically from convection in an atmosphere with shear using a second-order WKBJ approximation. We calculate the accelerations these waves impart to the atmosphere as a function of altitude by taking the divergence of the gravity wave momentum flux. In our work, the divergences can result either from wavebreaking or absorption at critical layers. We expect similarities between these two loss mechanisms since waves are thought to break as they approach critical layers. Lastly, we develop analytic approximations in order to calculate wavebreaking divergences and to explain the WKBJ results.

We chose to use an analytic technique because it gives us the capability to track a broad spectrum of waves in three dimensions. Whereas it cannot offer much insight into detailed nonlinear interactions, nevertheless, we can model some of the nonlinear behavior analytically. In the end, it is more important for us to qualitatively understand the spectrum of gravity waves emitted from the convection over a large range of horizontal phase speeds.

In this paper we intend to address only one way in which dry convection can excite internal gravity waves. Other mechanisms can enter, for instance, if a substantial zonal wind shear lies within the convection, or if the convection can penetrate into the stable layer. Even though these mechanisms can be efficient, evidence does not exist to support their presence in Venus's middle atmosphere.

This paper is divided into four parts. The first is this introduction. In the second we present the analytic theory for the generation and propagation of internal gravity waves. In the third we present WKBJ results. We include order of magnitude estimates and analytic approximations of some of these results. Finally, in the fourth section we present conclusions and a discussion of practical implications.

2. Formulation

The goal of this section is to calculate the momentum flux carried by waves generated by turbulent convection and to show how the momentum is eventually deposited in the atmosphere.

a. The wave generation equation

We use the anelastic equations (Ogura and Phillips 1962) in order to omit compressional effects and to include nonhydrostatic effects. We retain terms in the anelastic equations that account for zonal winds and static stability, which vary in altitude. The anelastic equations are

$$\frac{du}{dt} = -\frac{\partial \phi}{\partial x} \tag{1a}$$

$$\frac{dv}{dt} = -\frac{\partial \phi}{\partial y} \tag{1b}$$

$$\frac{dw}{dt} - \frac{g_v}{c_p} S = -\frac{\partial \phi}{\partial z} \tag{1c}$$

$$\frac{\partial u}{\partial x} + \frac{\partial v}{\partial y} + \rho^{-1} \frac{\partial}{\partial z}(\rho w) = 0 \tag{1d}$$

$$\frac{dS}{dt} = 0. \tag{1e}$$

In these equations, ϕ is the Gibbs free energy plus the gravitational potential (π in Ogura and Phillips), S is the specific entropy, g_v is the gravitational acceleration, ρ is the mass density, c_p is the specific heat at constant pressure, u and v are winds in the horizontal plane, w is the vertical wind, and x, y, and z are the corresponding coordinates. The x coordinate increases to the east although the background zonal wind is westward. Thus, the mean zonal wind $\bar{u}$ and the zonal wind gradient in altitude $d\bar{u}/dz$ are negative in Venus's middle atmosphere. The density ρ is an independently determined function of z and is considered a background property of the atmosphere. The time derivatives are fully advective, meaning that $d/dt \equiv \partial/\partial t + \mathbf{u}\cdot\nabla$, where $\mathbf{u}$ is the wind field given by (u, v, w).

We assume a vertically finite convection layer between roughly 50- and 55-km altitude with an overlying atmosphere of variable background wind and static stability. Within the convective layer, there is no static stability and no shear in the zonal winds. Even though we shall initially examine wave generation in a simplified atmosphere, ultimately we shall use profiles that describe Venus's middle atmosphere.

Following GK, we find the wave generation equation for ϕ by separating the variables into a mean state and a fluctuation. We accomplish this by setting $u = \bar{u}(z) + u_c + u'$, $v = v_c + v'$, $w = w_c + w'$, $\phi = \bar{\phi}(z) + \phi_c + \phi'$, and $S = \bar{S}(z) + S_c + S'$. The barred quantities are the mean-state quantities and are constant in time. The quantities with a subscript "c" are associated with convective motions and are nonzero only in the convecting layer. The primed quantities are the fluctuations associated with wave motions and are small compared to the quantities associated with convective motions. We define

$$N^2(z) \equiv \frac{g_v}{c_p}\frac{d\bar{S}}{dz},$$

which is the square of the Brunt–Väisälä frequency.

The wave fluctuation terms are Fourier transformed using an $\exp[i(\omega t - k_x x - k_y y)]$ dependence. We assume that there is no zonal wind shear ($\partial\bar{u}/\partial z = 0$) and no static stability ($N^2 = 0$) in the convecting layer because of vigorous mixing of momentum and entropy by the convection. We then find a vertical structure equation for the ω, k_x, k_y Fourier component of the Gibbs free energy fluctuation ϕ':

$$\frac{\partial}{\partial z}\left(\frac{\bar{\rho}}{N^2 - \tilde{\omega}^2}\frac{\partial \phi'}{\partial z}\right) + \frac{\bar{\rho}k^2}{\tilde{\omega}^2}\phi' = \frac{1}{\tilde{\omega}^2}(F^{(1)} + F^{(2)}). \tag{2}$$

We have used the following definitions:

$$\omega_D(z) \equiv \omega - k_x(\bar{u}(z) - \bar{u}(\text{convection})) \tag{3a}$$

$$k^2 \equiv k_x^2 + k_y^2 \tag{3b}$$

$$\tilde{\omega}(z) \equiv \begin{cases} \omega_D(z) - i/\tau_c & \text{within the convection,} \\ \omega_D(z) & \text{outside the convection.} \end{cases} \tag{3c}$$

The quantity ω_D is the Doppler frequency, and the quantity τ_c is a time constant associated with convective reabsorption. Its magnitude is dependent on the horizontal scale of the waves in a manner laid out later in this section. As long as τ_c is finite, the quantity $\tilde{\omega}$ is discontinuous at the interface between the convecting layer and the stable layer. The nonhomogeneous wave generation terms are

$$F^{(1)} = \nabla\cdot\nabla\cdot(\bar{\rho}\mathbf{u}_c\mathbf{u}_c) \tag{4a}$$

$$F^{(2)} = -\frac{\partial}{\partial z}\left(\frac{\bar{\rho}gS_c}{c_p}\right). \tag{4b}$$

In the terms $F^{(1)}$ and $F^{(2)}$, $\mathbf{u}_c$ is the convective wind velocity field, and S_c is the entropy fluctuation associ-

ated with the convection. Both of these terms arise from nonlinear terms in the anelastic equations. The forcing terms are the same as those found and discussed in GK. For a nearly adiabatic background atmosphere (Ogura and Phillips 1962), we find that

$$\phi' = \frac{p'}{\bar{\rho}}. \tag{5}$$

In deriving (2) from the anelastic equations (1), we anticipate that the wave fluctuation terms are negligible compared to their convective equivalents (c.f. Lighthill 1952; Stein 1967). This allows us to separate the two types of fluctuations such that wave fluctuations are on the left-hand side of (2) and the convective fluctuations are on the right-hand side of (2). The amplitude of the convective motions, and hence the nonhomogeneous terms, can be adequately described by the mixing length hypothesis (Schwarzschild 1958) with a Kolmogorov spectrum and high spatial and temporal frequencies. On the other hand, the horizontal wind fluctuations u', v' and u_c, v_c are all the same order of magnitude. This exception implies that 1) the convective motions can damp the wave motions, and 2) the wave motions can partially "organize" the convective motions. We implement the former implication by including a convective reabsorption time constant τ_c. We neglect the latter implication because little is known about it even though it has been seen in numerical models (Fovell et al. 1992).

We neglect viscous and radiative damping of the wavelike fluctuations. Lindzen and Forbes (1983) have shown that damping by eddy viscosity where gravity waves break reduces wave amplitudes to the point where they are no longer unstable. Thus, we include the main effect of eddy viscosity by requiring that with wavebreaking the waves never exceed saturation. Otherwise, we neglect eddy viscosity. Crisp (1989) showed that the radiative damping times for disturbances with vertical scales of 7 km is on the order of a few Earth days, which would be significantly less efficient than any damping resulting from wavebreaking.

In order to evaluate wave amplitudes and their vertical propagation characteristics, we must solve (2), which is a one-dimensional nonhomogeneous differential equation in z. Given upper and lower boundary conditions, we can analytically solve for the vertical structure of ϕ' for any choice of ω, k_x, and k_y.

b. The solution

Since the convection is a nonlinear random phenomenon, we treat it statistically as a stationary random process. We can solve for ϕ' in a statistical sense given the statistical properties of F. In mathematical notation, $B_\phi(\omega, k_x, k_y; z)$, the spectral variance of $\phi'(z)$, will be found in terms of $B_F(\omega, k_x, k_y)$, the spectral variance of the forcing. Consequently, u' and w' cannot be calculated individually, but the momentum flux spectrum $\bar{\rho}\,\overline{u'w'}(\omega, k_x, k_y)$ can be.

The spectral variance notation is useful for describing properties of random processes. In general, the quantity $B_\chi(a; z)$ is a variance spectrum of χ' in a as a function of z. For example, the quantity $B_T(\omega; z)\,d\omega$ is the amount of variance of the temperature fluctuations T' at altitude z in the spectral interval between ω and $\omega + d\omega$. The result would have the units of degrees squared. All quantities on the left side of the semicolon within the parentheses are spectral coordinates. The variance also depends on the coordinates on the right side of the semicolon, but not in an integral sense. For a more detailed exposition on the mathematics of random processes see Ishimaru (1978).

We find the solution to the wave generation equation using a conventional technique for second-order nonhomogeneous differential equations with boundary conditions (Morse and Feshbach 1953):

$$\phi' = h(z) \int_{\text{convection}} dz' \, \frac{g(z')\tilde{\omega}^{-2}F(z')}{\bar{\rho}(N^2 - \tilde{\omega}^2)^{-1}\,\mathrm{Wr}(g, h)}. \tag{6}$$

This solution holds above the convecting layer; a slightly different solution holds below it. Here, $F(z)$ is the Fourier transform in frequency ω and horizontal wavenumbers k_x, k_y of the sum of the two forcing terms $F^{(1)}$ and $F^{(2)}$ as a function of altitude z within the convection. In the neutrally buoyant convection, $N^2 = 0$ and $\tilde{\omega}^2 = (\omega - i/\tau_c)^2$. The forcing term F is nonzero only in the convecting layer, which is embedded in the neutrally buoyant layer. The functions $g(z)$ and $h(z)$ are homogeneous solutions to the wave equation for which $g(z)$ satisfies a boundary condition at the lower boundary and $h(z)$ at the upper boundary. The Wronskian of $g(z)$ and $h(z)$ is given by

$$\mathrm{Wr}(g, h) = g\left(\frac{\partial h}{\partial z}\right) - h\left(\frac{\partial g}{\partial z}\right). \tag{7}$$

The product of $\mathrm{Wr}(g, h)$ with the quantity $\rho/(N^2 - \tilde{\omega}^2)$, the product being the denominator of the integrand of (6), is independent of height. Thus, it is only necessary to calculate the denominator at one convenient altitude.

c. Homogeneous solutions

We solve the homogeneous portion of (2) to find the solutions $g(z)$ and $h(z)$. We use the WKBJ approximation. This approximation requires that the vertical wavelength be much smaller than the vertical scale over which it varies. This condition does not always hold, and therefore the complete theory incorporates connection formulas for those regions in which the WKBJ conditions fails.

Two continuity conditions are required for the Gibbs free energy fluctuations and the related functions $g(z)$

and $h(z)$. We require that ϕ' and w' be continuous in z so that pressure gradients and mass flux divergences remain finite. The vertical wind fluctuation is given in terms of ϕ' as

$$w' = \frac{-i\tilde{\omega}}{N^2 - \tilde{\omega}^2} \frac{\partial \phi'}{\partial z}. \quad (8)$$

Continuity of w' amounts to continuity in $\partial\phi'/\partial z$ except where $\tilde{\omega}$ is discontinuous [c.f. (3c)].

The WKBJ solution has wavelike solutions with a vertical wavenumber $m(z)$, which is given by the well-known internal gravity wave dispersion relation (Bretherton 1966):

$$m^2(z) = \left[\frac{N^2(z)}{\tilde{\omega}^2(z)} - 1\right] k^2. \quad (9)$$

The terms on the order of the square of the inverse scale height are absent in the second-order WKBJ theory because the explicit WKBJ condition is that $mH \gg 1$. Neglecting terms of order $1/H^2$ is valid even when near a turning point. Since the static stability and the zonal wind vary over vertical scales on the order of a scale height, we expect the vertical wavenumber m to vary over vertical scales on the order of a scale height. The WKBJ solution for $mH \gg 1$ is

$$\phi'_{\text{homogeneous}} \approx \tilde{\omega}\sqrt{\frac{m}{\bar{\rho}}}\,(c_1 e^{iq} + c_2 e^{-iq}), \quad (10)$$

where the phase of the wave q is defined from some arbitrary altitude z^* as

$$q \equiv \int_{z^*}^{z} |m(z')|\, dz' \quad (11)$$

and c_1 and c_2 are general coefficients. We usually define z^* as the altitude of a particular turning point. Turning points occur where $m^2(z^*) = 0$. The coefficients c_1 and c_2 are specifically associated with the turning point at altitude z^*.

When $\tilde{\omega}^2 > N^2$, the vertical wavenumber squared, m^2, becomes negative and the solutions are exponential growth and decay in the depth q:

$$\phi'_{\text{homogeneous}} \approx \tilde{\omega}\sqrt{\frac{|m|}{\bar{\rho}}}\,(c_3 e^{q} + c_4 e^{-q}), \quad (12)$$

where q retains the definition of (11) and $m(z')$ is imaginary. The coefficients c_3 and c_4 are specifically associated with the turning point at altitude z^*. For every choice of ω, k_x, and k_y, both exponential and wavelike regions of behavior will occur. The WKBJ solutions (10) and (12) break down where $m^2 \to 0$, between regions of sinusoidal and exponential behavior. Connection formulas are used to tell us the behavior of the homogeneous solutions in such regions. We derive the connection formulas and show how they are used in constructing the homogeneous solution $h(z)$ in appendix A.

1) THE HOMOGENEOUS SOLUTION $h(z)$

The function $h(z)$ gives the vertical structure of an individual wavemode above the region of forcing. Depending on ω, k_x, and k_y, one can get a variety of wave cases when N^2 and $\bar{u}$ vary with height. We can get waves that have only an upward propagating component and thus "radiate" their energy to space (*propagating* waves), waves that have equal upward and downward propagating components and are thus trapped beneath a reflection layer in a horizontal duct (*trapped* waves), waves that lose all their energy at a critical layer (where $\omega_D = 0$) (another type of *propagating* wave), or no waves at all. Here we discuss how the different wave cases arise and how they are implemented in our theory.

Most prograde waves (i.e., those propagating horizontally in the direction of the mean flow—westward) are propagating waves. We adopt the convention $\omega > 0$, so prograde waves have $k_x < 0$. Prograde waves whose westward phase speeds are smaller than the maximum westward wind speed, which is about 60 m s^{-1} with respect to the convection, are critically absorbed. Critical absorption arises because $\tilde{\omega}$ decreases with height and becomes zero at some altitude above the convection [see (2)]. We regard waves that propagate directly into a critical layer as *propagating* waves because the energy they carry from the convection never returns to the convection (valid for large Richardson number flows such as Venus's). Even though waves with prograde zonal phase speeds larger than about 60 m s^{-1} do not encounter critical layers, it turns out that such waves have very little energy and momentum associated with them. For propagating waves, we require radiation to space as the upper boundary condition [i.e., $c_2 = 0$ in (10)].

While prograde modes are all propagating, retrograde (eastward) modes are either propagating or trapped. Retrograde waves have $k_x > 0$, so $\tilde{\omega}$ increases with height. If $\tilde{\omega}$ grows rapidly enough so that a region of nonpropagation forms ($\tilde{\omega}^2 > N^2$) where the zonal wind peaks, a vertically restricted wave, called a trapped wave, forms as long as a region of propagation ($\tilde{\omega}^2 < N^2$) remains between 55 and 66 km. We refer to the region of nonpropagation, which forms around 66 km, as the *upper lid.* For trapped waves, we impose perfect reflection as the upper boundary condition by setting $c_1 = c_2 \exp(\pi i/2)$ for the turning point at the base of the upper lid [see (10)].

Figure 1 illustrates the basic features of $h(z)$. In this figure we show how the Doppler frequency ω_D and the Brunt–Väisälä frequency together allow propagating and trapped modes. We have chosen two different modes, one an example of a propagating/critically ab-

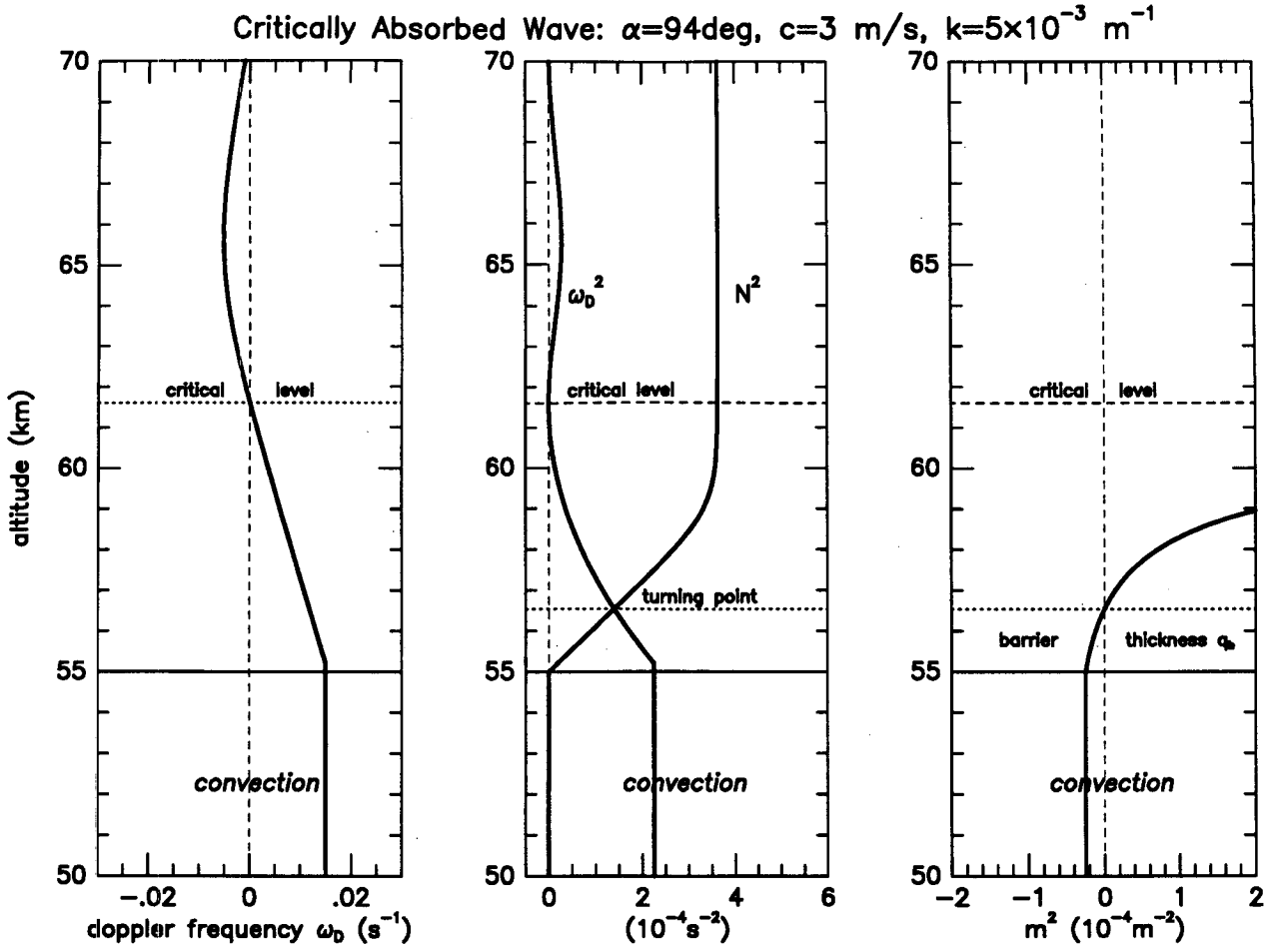

FIG. 1. Different wave cases. In these panels we show profiles of the Doppler frequency, the square of the Doppler frequency, the square of the Brunt–Väisälä frequency, and the square of the vertical wavenumber for (a) a critically absorbed "propagating" wave, and (b) a "trapped" wave. For (a) we use $\omega = 1.5 \times 10^{-2}$ s^{-1}, $k_x = -3.49 \times 10^{-4}$ m^{-1}, and $k_y = 4.99 \times 10^{-3}$ m^{-1}. For (b) we use $\omega = 9.6 \times 10^{-3}$ s^{-1}, $k_x = 2.74 \times 10^{4}$ m^{-1}, and $k_y = 7.52 \times 10^{-4}$ m^{-1}.

sorbed mode and the other an example of a trapped mode. Turning points occur where $\tilde{\omega}^2 = N^2$ [see (2)].

2) THE HOMOGENEOUS SOLUTION $g(z)$

The homogeneous solution $g(z)$ serves two purposes in this problem: it allows us to project the wavemode onto the forcing mechanism and to calculate the forcing efficiency for each mode through evaluation of the Wronskian of $g(z)$ with $h(z)$. For these reasons, we only need to know the functional form of $g(z)$ below $z = 55$ km. In order to retain mathematical simplicity, especially for $k < 1/H$, we assume that the convection is Boussinesq. This is a good approximation for small scales ($kH \gg 1$) and is a fair approximation for all scales, since the convection is no more than one scale height deep. In the Boussinesq case, $d\bar{\rho}/dz$ is zero, and $g(z)$ is a combination of growing and decaying exponentials of kz.

We assume that below the convection the atmosphere is stable with a constant Brunt–Väisälä frequency. With any substantial stability, we argue that the stable layer essentially inhibits vertical wind fluctuations, creating a "solid" lower boundary ($\partial g/\partial z = 0$) to downward wave radiation. Thus, we approximate the functional form of $g(z)$ as $\cosh k(z - z_{\text{bottom}})$, where z_{bottom} is the altitude of the bottom of the convecting layer. Our argument does not imply that emission of gravity waves into the stable lower layer will not occur, only that the emission of waves into the lower layer should not affect the emission of waves into the upper layer, the one with which we are concerned. Thus, in our problem we define

$$g(z) \equiv \cosh k(z - z_{\text{bottom}}), \tag{13}$$

where H is approximately $z_{\text{top}} - z_{\text{bottom}}$.

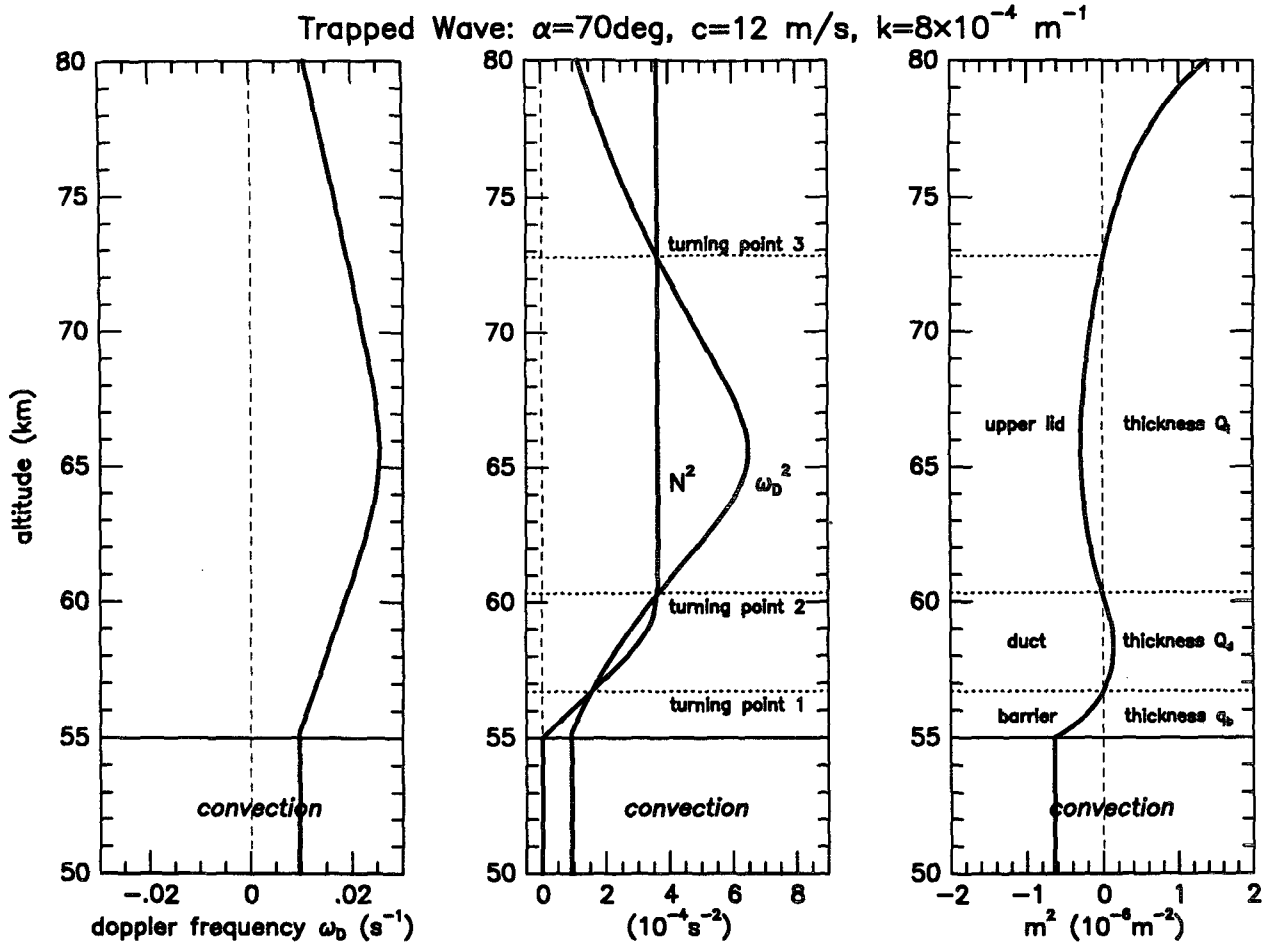

FIG. 1. (*Continued*)

d. The Wronskian Wr(g, h)

The Wronskian $\mathrm{Wr}(g, h)$ is given by (7). For simplicity, we choose to evaluate the Wronskian at $z = z_{\mathrm{top}} - \epsilon$ (z_{top} is the altitude of the top of the convecting layer, and ϵ is some infinitesimal distance). It uses the boundary conditions in order to describe the response of the waves to forcing. Because of convective reabsorption, $\tilde{\omega}$ is a complex number within the convecting layer; therefore, the Wronskian is always nonzero.

Throughout this calculation it is necessary to compute the derivatives of $h(z)$ and ϕ' with respect to height. A simple finite difference is inappropriate since it would introduce third-order WKBJ terms even though we only desire second-order accuracy. Although third-order terms are small, nonetheless, we require certain cancellations to occur at all orders in the vicinity of turning points. The proper way to find the derivatives of $h(z)$ and ϕ' with respect to z is to find the second-order WKBJ solution for $\partial h/\partial z$ independently. We show how this is done in appendix B.

e. The forcing

Since we desire that the final result of this calculation give a variance spectrum of a random process, we must relate our eventual solution to variance properties of the forcing terms F given in (4). To find the variance of ϕ', we multiply (6) by its complex conjugate. The result is

$$B_\phi(\omega, k_x, k_y; z) = \frac{|h(z)|^2}{|\mathrm{Wr}|^2}\,\mathcal{C}(\omega, k_x, k_y), \quad (14a)$$

where

$$\mathcal{C}(\omega, k_x, k_y) = \iint g(z')g(z'')\overline{F(z')F^*(z'')}\,dz'dz''. \quad (14b)$$

The overbar denotes an ensemble average, and the F's depend on ω, k_x, and k_y. The integrals are calculated over the depth of the convection in which $N^2 = 0$. We will find that many quantities are dependent on a quantity M, which is related to $\mathcal{C}$ through

$$M(\omega, k_x, k_y) = \frac{\mathcal{C}(\omega, k_x, k_y)}{|\mathrm{Wr}|^2}. \quad (15)$$

Next we must calculate the integrals over the depth of the convection.

In calculating $\mathcal{C}(\omega, k_x, k_y)$, we first assume that the two forcing terms of (4) are statistically uncorrelated. Second, we assume that each term is correlated when $|z' - z''| \leq 1/k$ and is uncorrelated otherwise. Third, the forcing terms have no amplitude at the upper and lower boundaries of the convection. With these assumptions we now approximate the integrals of (14b).

We do the integrals of (14b) by parts. The partial derivatives are removed from the forcing terms and are instead applied to $g(z')$ and $g(z'')$. The boundary terms are zero because of our last approximation listed above. We use (13) to evaluate $g(z')$ and $g(z'')$. When $kH \gg 1$, the g's decay exponentially with depth into the convection, and the integral is

$$\mathcal{C}(\omega, k_x, k_y) \approx k^2 B_{w_c^2}(\omega, k_x, k_y) + \left(\frac{g_v}{c_p}\right)^2 B_{S_c}(\omega, k_x, k_y), \quad (16)$$

where c_p is the specific heat at constant pressure and g_v is the gravitational acceleration. On the other hand, when $kH \ll 1$, the g's and the F's extend over the depth of the convection. Upon integrating by parts and using the expression (13) for both g's, we find that

$$\mathcal{C}(\omega, k_x, k_y) \approx (k \tanh kH)^2 B_{w_c^2}(\omega, k_x, k_y) + (\Delta g)^2 (g_v^2/c_p^2) B_{S_c}(\omega, k_x, k_y), \quad (17)$$

where Δg is the difference in $g(z)$ from the top to the bottom of the convection. This difference is given by

$$\Delta g = 1 - \operatorname{sech} kH. \quad (18)$$

Since the high kH limit of (17) gives the same result as (16), we use (17) as our best approximation for $\mathcal{C}(\omega, k_x, k_y)$ throughout the rest of our work.

f. Variance properties of the turbulence

The amplitude of the convective fluctuations will determine the overall amplitude of the momentum flux spectrum of the convectively generated waves. Here we show how this amplitude is determined.

The Reynolds-type and entropy-type forcing terms of (4) are related by mixing length theory. As shown by GK, these two terms have the same order of magnitude for the largest convecting eddies. This is because the work done by a parcel with an entropy fluctuation S_c after traveling a vertical distance H is roughly the same as the kinetic energy it releases. Thus, $g_v H(S_c/c_p) \sim W_c^2$, where W_c is the typical wind speed of a large eddy. The largest convective wind speeds measured by the VEGA balloons were on the order of 3–5 m s^{-1}, so we choose W_c in this range. This is in good agreement with the value obtained by estimating the convective energy flux as $\rho W_c^3 \approx 40$ W m^{-2}, with $\rho = 1.5$ kg m^{-3} and $W_c = 3$ m s^{-1} (Ingersoll et al. 1987).

At small scales and high frequencies, we parameterize the forcing by connecting the mixing length hypothesis with a Kolmogorov energy cascade (Landau and Lifshitz 1987; Lumley and Panofsky 1964). The kinetic energy spectrum $(1/2)B_w(k)$ is the familiar $k^{-5/3}$ of Kolmogorov theory. In two dimensions it is $(1/2)B_w(k_x, k_y) \propto k^{-8/3}$, valid for $kH \gg 1$. These power law relations are derived by assuming the spectral density B_w depends only on the energy dissipation rate ϵ and on k. Since ϵ has dimensions of l^2t^{-3}, where l is a length and t is a time, and $B_{w_c^2}(k_x, k_y)$ has dimensions of (velocity)^4 per (wavenumber)^2, we have $B_{w_c^2}(k_x, k_y) \sim \epsilon^{4/3}k^{-10/3}$ at $kH \gg 1$.

At high ω (frequency) the dependence is more uncertain. We define τ_k as the correlation time constant for eddies of size $1/k$. For large horizontal scales, τ_k is of order H/W_c. At small scales it represents the time it takes the large eddies to advect parcels a distance $1/k$. An expression consistent with both of these limits is

$$\frac{1}{\tau_k} = \frac{W_c}{H_c}(1 + k^2H^2)^{1/2}. \quad (19)$$

The quantity $B_{w_c^2}(\omega)$ has dimensions of (velocity)^4 per (frequency). The combination $\epsilon^2\omega^{-3}$ has these dimensions. Combining the $k^{-10/3}$ and ω^{-3} dependences at high k and high ω, we get

$$B_{w_c^2}(\omega, k_x, k_y) = \frac{1}{3\pi} \frac{W_c^4 H_c^2}{[1 + (kH_c)^2]^{5/3}} \frac{\tau_k}{[1 + (\omega\tau_k)^2]^{3/2}}. \quad (20)$$

The factor of $1/(3\pi)$ is a normalization constant such that the integral of the above quantity over all ω, k_x, and k_y is W_c^4.

As shown by Lumley and Panofsky (1964, p. 85), the variance spectrum of entropy is different from that of w_c^2 because S_c is a passive scalar fluctuation: it has no significant effect on the motion for these small scales and high frequencies. The entropy fluctuations have their own dissipation rate ϵ_s, which has the dimensions (entropy)^2 per time. We assume that the variance spectra B_{S_c} depend only on ϵ_s, ϵ, k, and ω. Thus, $B_{S_c}(k_x, k_y)$ has dimensions (entropy)^2 per (wavenumber)^2 and varies as $\epsilon_s\epsilon^{-1/3}k^{-8/3}$ at $kH \gg 1$. Likewise, the quantity $B_{S_c}(\omega)$ has dimensions (entropy)^2 per frequency and varies as $\epsilon_s\omega^{-2}$ for $\omega \gg (W_c/H)$. Combining these and using $g_v H(S_c/c_p) \sim W_c^2$, we obtain

$$B_{S_c}(\omega, k_x, k_y) = \frac{1}{3\pi^2} \frac{c_p^2}{(gH)^2} \frac{W_c^4 H_c^2}{[1 + (kH_c)^2]^{4/3}} \frac{\tau_k}{1 + (\omega\tau_k)^2} \quad (21)$$

for the spectrum of S_c, where H_c denotes the horizontal correlation length of the energy bearing eddies ($H_c \approx H$ for nearly isotropic turbulence).

Equations (20) and (21) may overestimate the amplitude in the limit $k \to 0$, ω finite. These modes have large horizontal speeds, faster than the convective velocity W_c. It is not certain that such modes exist in the convection. Such fast-moving waves could, in principle, propagate to the height of the zonal wind maximum without encountering a critical layer and might provide a significant momentum source at that altitude. As we shall see, the net momentum source at that altitude is negligible according to our theory. So apparently these modes are not important. The fact that they are allowed by (20) and (21) does not affect our conclusions.

It would be possible to generate higher phase speeds if the horizontal correlation length of the convective eddy motions were larger and their coherence time remained the same. Large convective cells are apparent in some regions of Venus's atmosphere (Belton et al. 1976). We believe that these are not isolated to the 5-km convective layer sensed by the VEGA balloons and that they are more likely signatures of deeper convection. In this paper we choose to address waves generated by convective eddies vertically confined within the deep cloud, which are most likely roughly isotropic in scale.

g. *Momentum flux*

The momentum flux is broken down by wavemode in the same way as the Gibbs free energy variance. An individual wavemode of frequency ω and horizontal wavenumbers k_x and k_y will contribute a momentum flux at $\bar{\rho}\,\overline{u'w'}(\omega, k_x, k_y)$, which is defined such that $\bar{\rho}\,\overline{u'w'}(\omega, k_x, k_y)d\omega dk_x dk_y$ is the amount of momentum flux in the Fourier volume $d\omega dk_x dk_y$. We relate u' and w' to ϕ' and $\partial\phi'/\partial z$, which we get from h and $\partial h/\partial z$ (appendices A and B), to show that

$$\bar{\rho}\,\overline{u'w'}(\omega, k_x, k_y) = \frac{k_x}{2} k^2 M(\omega, k_x, k_y), \quad (22)$$

where $M(\omega, k_x, k_y)$ is given by (15). We note that this quantity is independent of height outside regions of forcing, wavebreaking, and critical layers, consistent with noninteraction theorems (Andrews and McIntyre 1976).

There are two other conserved second-order quantities associated with propagating internal gravity waves: the wave action flux and the energy flux. We denote the wave action flux for each given mode as $\mathcal{A}(\omega, k_x, k_y) \equiv \bar{\rho}\,\overline{\phi'\omega'}(\omega, k_x, k_y)/\tilde{\omega}$ (e.g., Andrews et al. 1987) and the energy flux as $\mathcal{E}(\omega, k_x, k_y) \equiv \bar{\rho}\,\overline{\phi'w'}(\omega, k_x, k_y)$. The energy flux according to this definition is not conserved with height because the wave interacts with the mean flow. Nonetheless, the actual energy carried by a wave can be calculated by the above definition at the location of its generation; thus, $\tilde{\omega} = \omega$. Using the linearized anelastic equations (1) for u', w', and ϕ' [or (3.7) in Booker and Bretherton 1967], we find the wave action flux $\mathcal{A}$ and the energy flux $\mathcal{E}$ are

$$\mathcal{A}(\omega, k_x, k_y) = \frac{k^2}{2} M(\omega, k_x, k_y) \quad (23)$$

and

$$\mathcal{E}(\omega, k_x, k_y) = \frac{\omega k^2}{2} M(\omega, k_x, k_y). \quad (24)$$

h. *Wavebreaking*

We know from previous work that gravity waves break throughout Earth's atmosphere and there is no reason to assume that the same does not happen on Venus. In fact, gravity waves are known to break before they ever reach their critical layers (Geller et al. 1975), so we assume that wavebreaking is chiefly responsible for the deposition of momentum by the waves.

We assume that waves break just enough so that they are only barely stable against the convective instability condition. Waves can break because of Kelvin–Helmholtz instabilities and convective instabilities, but it was shown that the convective instability dominates for waves in a nonshearing flow (Hodges 1967; Hines 1991). The convective instability criterion is also sufficient in a shear flow provided that the background Richardson number is much larger than 1/4. This criterion holds that the temperature fluctuations at any vertical-scale size ($dm \sim m$) associated with the waves cannot exceed the stability of the atmosphere (given in Kelvins per kilometer). Mathematically this is written as

$$B_T(m) \leqslant \frac{\Gamma^2}{m^3}, \quad (25a)$$

where

$$\Gamma \equiv (dT/dz)_{\text{atmosphere}} - (dT/dz)_{\text{adiabat}}.$$

For a Richardson number of order unity, this spectrum is equivalent to the "saturated" spectrum (Dewan and Good 1986; Smith et al. 1987), which is

$$B_u(m) + B_v(m) \leqslant \frac{N^2}{m^3}. \quad (25b)$$

The saturated spectrum has been observed in Earth's atmosphere at vertical scales between 10 m and a few kilometers.

At this point, we have laid out how our problem is solved numerically. Given background profiles of $\bar{u}(z)$ and $N^2(z)$, we can compute a three-dimensional spectrum of gravity waves. We do so by first calculating the factor $M(\omega, k_x, k_y)$ for each mode using (15)–(18). The variance spectra B_{S_c} and $B_{\omega_c^2}$ are computed using (19)–(21). Momentum fluxes are then com-

puted using (22). Temperature fluctuation spectra are calculated using

$$B_T(\omega, k_x, k_y; z) = \left|\frac{\Gamma h_z}{N^2 - \tilde{\omega}^2}\right|^2 M(\omega, k_x, k_y). \quad (26)$$

This arises from multiplying the vertical displacement of a parcel by Γ.

3. Results

In this section we show the spectra for two models with the intention of deriving a realistic momentum flux spectrum. The first and simplest model consists of a stable layer with constant N^2 and no wind shear overlying a convective layer with thickness H. The second model has variable zonal wind and a variable static stability in the stable layer that mimic the background profiles of zonal wind and static stability of the Venus middle atmosphere. These two models are summarized by Fig. 2.

a. Model I

With this first model, we show that the low, horizontal phase-speed waves must break immediately upon emission from the convection and show how much momentum is carried by high horizontal phase-speed waves.

In this model the stability is fixed at $N^2 = 4.0 \times 10^{-4}\ s^{-2}$, typical for the stable layer high above the convection, and the wind is zero above the convecting layer. The background temperature profile is taken from the parameterization of Schubert and Walterscheid (1984). The pressure and density profiles are determined using the hydrostatic law in conjunction with the temperature profile. While choosing the profiles of N^2 and $\bar{T}$ independently is not entirely realistic, the model is useful for illustration purposes. The only type of wave possible in this model is propagating. For $\omega < 0.02\ s^{-1}$, waves propagate freely out of the convection without encountering a barrier. For ω

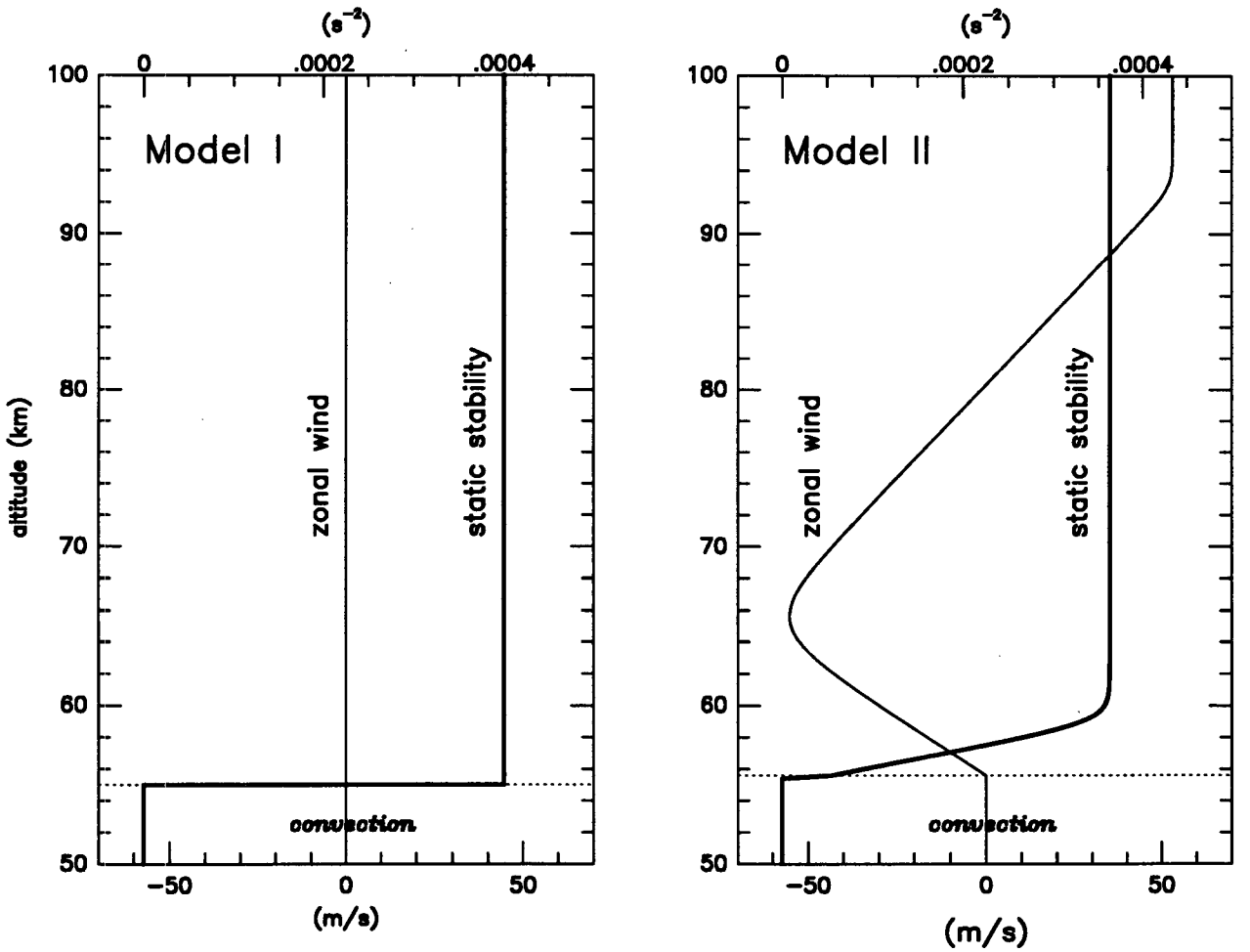

FIG. 2. Model wind and stability profiles. For the two models we show the static stability, or Brunt–Väisälä frequency N^2, and the zonal wind $\bar{u}$ as functions of altitude. The extent of the convecting layer is indicated.

$> 0.02\ s^{-1}$, the disturbances are evanescent and do not propagate.

We present a spectrum of temperature fluctuations at 60-km altitude, 5 km above the convection (Fig. 3), and momentum and energy fluxes at the point of emission (Fig. 4). Temperature variance spectra in vertical wavenumber are computed from $B_T(\omega, k_x, k_y)$ by integrating over two of the spectral parameters and choosing the other using (9) so that m is fixed. The most important phenomenon to appear in Fig. 3 is the growth of the temperature variance with increasing vertical wavenumber m for the "unbroken" waves. This is a manifestation of a strong singularity in the spectrum of gravity waves at low frequency. The singularity results from the factors of ω in the denominator of the right side of (2) and the existence of nonzero convective power at low frequency. This is evident at high vertical wavenumbers m in these spectra because m and ω are inversely proportional [see (9)]. In fact, according to Fig. 3, the spectrum of waves generated by the model without any breaking exceeds the saturated spectrum for vertical wavenumbers beyond a critical value of $0.01\ m^{-1}$. This condition holds at all levels, since N^2 and $\bar{u}$ are constant; therefore, we assume that the waves break as soon as they are emitted from the convection.

We call this process *breaking upon emission.* For use in the second model, where N^2 and $\bar{u}$ vary with height, we want a number that tells us what fraction of each wavemode survives breaking upon emission and is available for propagation to higher altitudes. This number, f_{breaking}, should depend only on properties of the wave and the convection but not on properties of the overlying atmosphere.

We first develop an approximate theory for the temperature variance spectrum immediately above the convection, before wave breaking has occurred. We start with (26) and (15) and use the definition of $h(z)$ for propagating waves given in appendix A. Taking into consideration the discontinuity of N^2 and $\tilde{\omega}$ across the

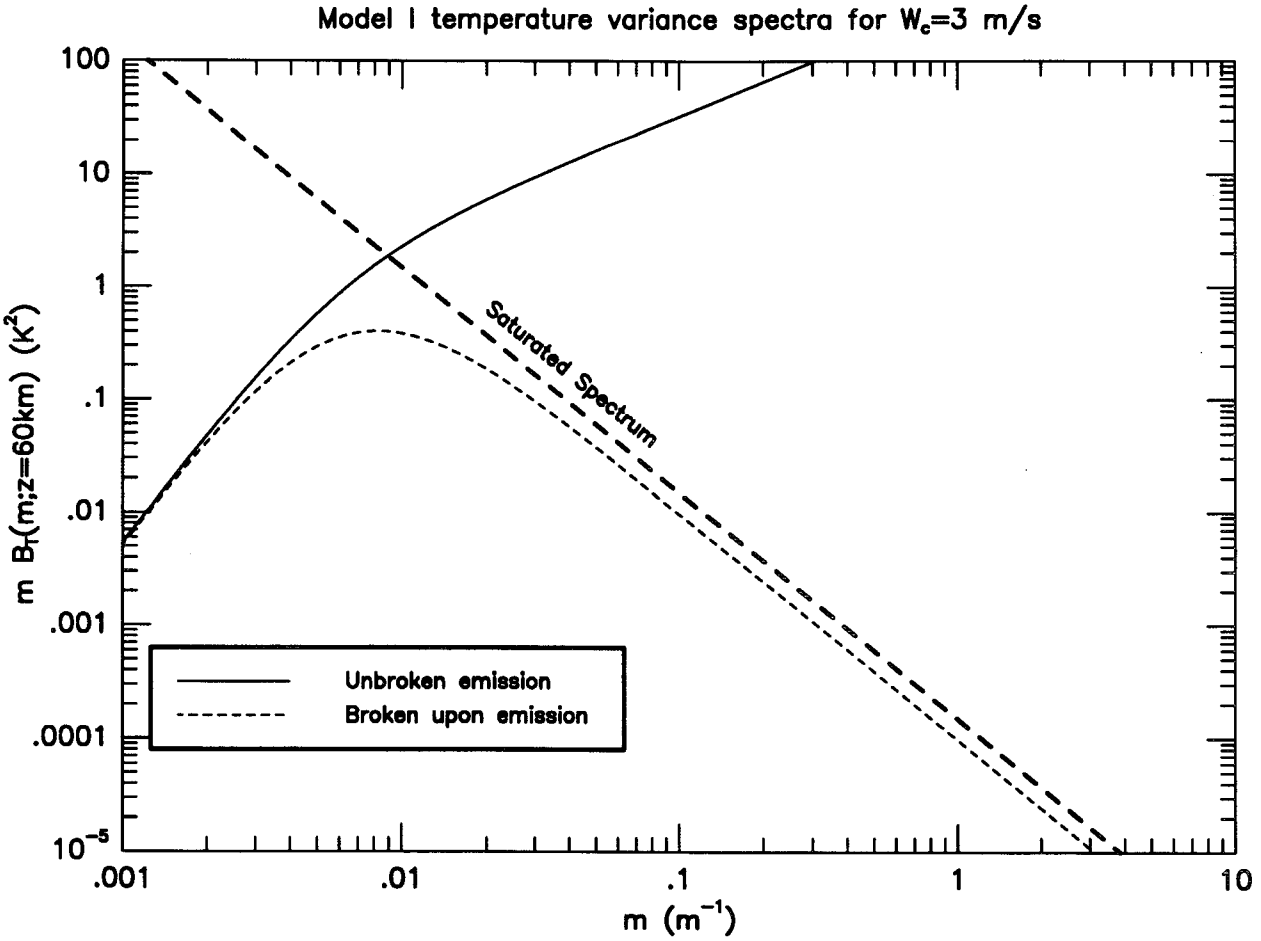

FIG. 3. Model I temperature variance spectra. We have plotted the temperature variance spectra in the log of the vertical wavenumber at 60-km altitude. Both types of forcing are represented for both unbroken and broken waves. We have taken $W_c = 3\ m\ s^{-1}$ and $H_c = 2 \times 10^{-4}\ m^{-1}$ for the forcing. Also present as the bold dashed line is the saturated spectrum as it is defined at 60 km ($\Gamma = 12.2\ K\ km^{-1}$).

interface between the convection and the stable atmosphere, we can evaluate the Wronskian just below the interface and get

$$\mathrm{Wr}(g, h) = \left(1 - \frac{i}{\omega\tau_c}\right)\left(\frac{\omega^2}{\omega^2 - N_c^2}\right) h_z(z = z_{\text{top}} + \epsilon) - k \tanh kH\, h(z = z_{\text{top}} + \epsilon). \quad (27)$$

Here, N_c is the value of N just above the interface. This Wronskian is dominated by the second term on the right at low frequencies, and thus $\mathrm{Wr} \sim h(z_{\text{top}})/H$. We approximate k_x, k_y, dk_x, and dk_y as $1/H$, and we assume $\omega \ll N$. Retaining the frequency dependence and using the relation

$$B_T(k_x, k_y, m; z) = \left(\frac{\partial\omega}{\partial m}\right)_{k_x,k_y} B_T(\omega, k_x, k_y; z),$$

we find that

$$B_T(m; z) \approx \frac{\rho_0}{\bar{\rho}(z)} \frac{N\bar{T}^2}{g_v^2} W_c^3. \quad (28)$$

Then f_{breaking} is simply the expression in (25a) for the saturated temperature variance spectrum divided by the expression in (28). The quotient is $f_{\text{breaking}} \approx (N/mW_c)^3$. Using the small phase speed approximation of the dispersion relation [see (9)] $m \approx N/c$, the breaking factor becomes $f_{\text{breaking}} = (c/W_c)^3$. This factor is only valid when it is less than unity. The saturated spectrum (25a) and the divergent spectrum (28) intersect at a critical vertical wavenumber given approximately by N_c/W_c (where N_c is the Brunt–Väisälä frequency directly above the convection). Waves with vertical wavenumbers greater than this critical wavenumber break, and those with vertical wavenumbers less than this critical wavenumber do not break; thus we define the breaking factor to be

$$f_e \equiv \frac{c^3}{(c^2 + W_c^2)^{3/2}}. \quad (29)$$

We show the effect of implementing this breaking factor in Fig. 3. In comparison with the saturated spectrum, the broken spectrum at wavenumbers larger than the critical wavenumber is smaller by a factor of 0.654 because the temperature variance spectrum of (28), which was used to define the breaking factor f_c of (29), is approximate.

For the first model we show "available" momentum and energy fluxes for $W_c = 3$ m s^{-1} in Fig. 4. The available fluxes are those carried by waves at the point of emission from the convecting layer after they have been broken upon emission. The ratio between the momentum flux and energy flux spectra is c_x [see (22) and (24)]. In the unbroken spectra, the infinity in the momentum flux spectra is another manifestation of the low phase speed singularity. Wavebreaking upon emission rids the momentum flux spectra of this singularity. After breaking upon emission, most of the energy and momentum appears to be carried by waves with phase speeds approximately given by W_c, consistent with GK.

We present a simple geometric argument to show how much momentum is transported vertically at zonal phase speeds much greater than W_c. First, we estimate the total momentum flux $\bar{\rho}\,\overline{u'w'}$ using (22) and the same assumptions involved in calculating $B_T(m)$:

$$\bar{\rho}\,\overline{u'w'} \approx \frac{\rho_0 W_c^3}{NH}. \quad (30)$$

We decompose this flux by the zonal phase speed c_x. The horizontal phase speed does not act like a vector. The zonal phase speed c_x is given by ω/k_x, whereas the *total* horizontal phase speed of the wave c is ω/k. It is possible to get very large zonal phase-speeds c_x for small values of the total phase speed c:

$$c_x = \frac{k}{k_x} c = c \sec\alpha,$$

where α is the angle at which the wave is propagating away from purely zonally. Thus, waves that have $\alpha \approx 90°$ have zonal phase speeds that are much larger than the phase speed c, which is of order W_c for the energy-bearing eddies. This suggests that even though most gravity waves will have small total phase speeds (much less than $\bar{u}$ at the zonal wind maximum), there may be enough that propagate meridionally in order to transport a significant amount of momentum to high altitudes in the presence of a strong wind shear.

If we assume that gravity waves are emitted isotropically from the convection, then $\bar{\rho}\,\overline{u'w'}(\alpha, c)$ must be proportional to $\cos\alpha$. In particular, we set

$$\bar{\rho}\,\overline{u'w'}(\alpha, c) = \frac{\mathcal{E}(\alpha, c)}{c} \cos\alpha$$

in which the quantity $\mathcal{E}(\alpha, c)$ is assumed independent of the angle α. The quantity $\mathcal{E}$ is actually the gravity wave energy flux given by a suitable integral of (24). Thus, we use $\mathcal{E}(\alpha, c) = \mathcal{E}(c)/2\pi$. We bin the momentum flux spectrum by c_x instead of by α and c by integrating

$$\bar{\rho}\,\overline{u'w'}(c_x) = \int_{-\pi/2}^{\pi/2} d\alpha \int_0^{c_x} dc\rho\,\overline{u'w'}(\alpha, c)\delta(c_x - c\sec\alpha)$$

in which we use $\delta(\ldots)$ to denote a Dirac delta function. After doing the integral over α, we find that the momentum flux spectrum in the zonal phase speed c_x is

$$\bar{\rho}\,\overline{u'w'}(c_x) = \frac{1}{\pi c_x^3} \int_0^{c_x} \frac{\mathcal{E}(c) c\, dc}{(1 - c^2/c_x^2)^{1/2}}. \quad (31)$$

If $\mathcal{E}(c)$ cuts off more rapidly than c^{-2} at high c, then the radical in (31) is unity for all c_x much larger than

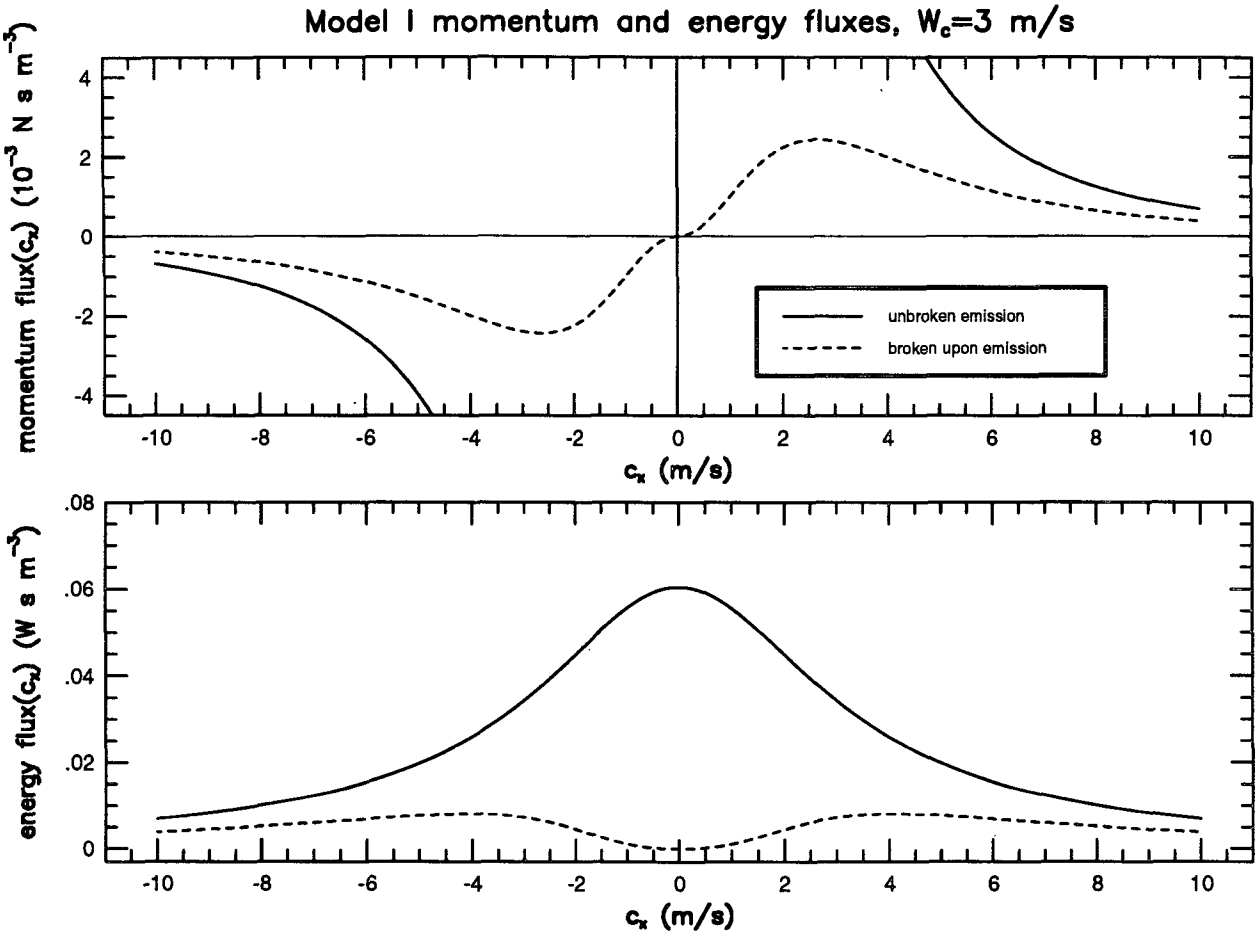

FIG. 4. Model I momentum and energy fluxes. In the top figure we show the momentum flux spectrum in zonal phase speed, $\bar{\rho}\,\overline{u'w'}(c_x)$, for waves unbroken and broken upon emission. In the lower figure we show the energy flux spectrum in zonal phase speed, $\mathcal{E}(c_x)$, for waves unbroken and broken upon emission.

the dominant phase speed c_0, and the momentum flux at high zonal phase speeds is

$$\bar{\rho}\,\overline{u'w'}(c_x) \approx \frac{1}{\pi c_x^3}\int_0^\infty \mathcal{E}(c)c\,dc.$$

Thus, although waves are emitted with high zonal phase speeds c_x, the momentum flux from these waves falls off as c_x^{-3}.

b. Model II

In the second model we implement the convective generation of gravity waves in an atmosphere that resembles that of Venus and show how the mean flow is accelerated by wave momentum deposition. We use profiles for $N^2(z)$ and $\bar{u}(z)$ in the same formulation as Schubert and Walterscheid (1984) with a few adjustments. We have made the entire region between 50 and 55 km neutrally buoyant because of the presence of convection in this layer in our model. We restrict the profile of $\bar{u}(z)$ above 55 km such that the Richardson number is never less than 1/4. The penetrative layer above the convection creates a discontinuity in N^2 at the interface between the convecting and stable layers. We set $N_c^2 = 4 \times 10^{-4}\ \mathrm{s}^{-2}$ at this interface by raising the top of the neutrally stable layer to 55.6-km altitude. Last, we implement breaking upon emission by redefining $M(\omega, k_x, k_y)$, which was previously given in (15), as

$$M(\omega, k_x, k_y) = \frac{\mathcal{E}(\omega, k_x, k_y)}{|\mathrm{Wr}|^2} f_e, \qquad (32)$$

where f_e is given by (29).

1) TEMPERATURE VARIANCE SPECTRA AND CRITICAL LAYER BREAKING

A typical temperature variance spectrum of waves broken upon emission is presented in Fig. 5 at an altitude of 60 km, about 5 km above the top of the con-

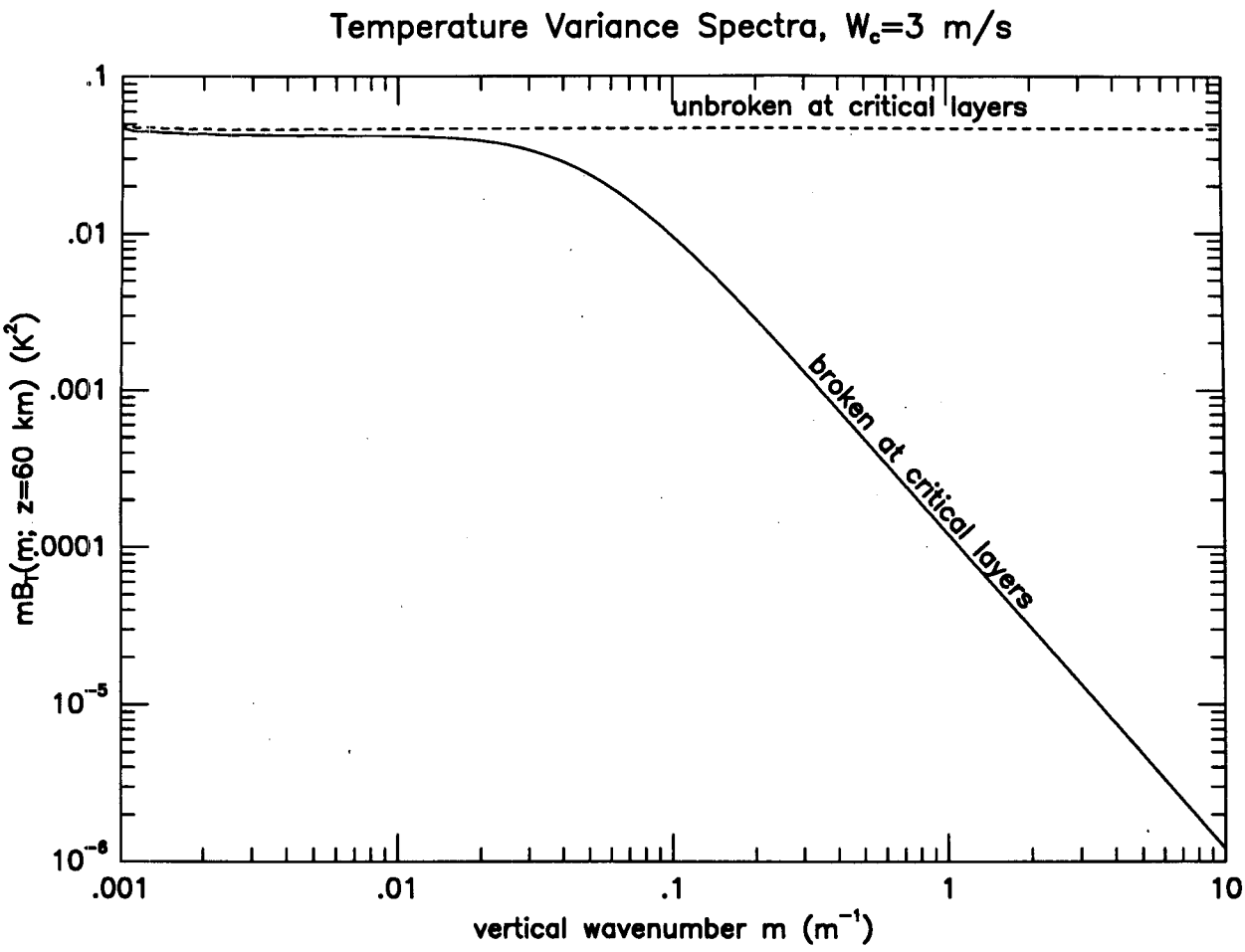

FIG. 5. Model II temperature variance spectra. We have plotted the temperature variance spectra in the log of the vertical wavenumber at 60-km altitude. Both spectra are broken upon emission. One of the spectra is unbroken near critical layers, and the other is broken near critical layers. The forcing intensity W_c is set to 3 m s^{-1}.

vecting layer. As each wavemode propagates toward its critical level z_c, where $\bar{u}(z_c) = c_x$, its vertical wavenumber increases. Without breaking, the temperature variance has finite density as $m \to \infty$ and is nonintegrable. We therefore need a breaking factor for critical layers, in addition to that for breaking upon emission.

We first develop an approximate expression for the unbroken temperature variance spectrum. We start with (26) and assume that emission is isotropic in the horizontal plane (i.e., $M(\omega, k_x, k_y) = M(\omega, k)/2\pi k$). We then transform $B_T(\omega, k_x, k_y)$ to ω, k, m coordinates. Since the waves that break will have large vertical wavenumbers, we assume that $k^2 \ll m^2$ and eliminate k^2 wherever it is additively paired with m^2. This allows us to replace every occurrence of $\tilde{\omega}$ with kN/m (an approximate form of the dispersion relation) while retaining occurrences of ω. Also, since the only waves that reach far above the convection are those that propagate obliquely to the mean flow, we approximate k_y as k. Putting all of these approximations together gives

$$B_T(\omega, k, m; z) \approx \frac{1}{4\pi} m^{-1} \frac{N^3 \bar{T}^2}{\bar{\rho}\,|\Delta u|\, g_v^2} k^2 M(\omega, k),$$

in which g_v is the gravitational acceleration and Δu is the difference in $\bar{u}(z)$ between the convecting layer and altitude z. Integrating this last equation over ω and k gives

$$B_T(m; z) \approx m^{-1} \frac{N^3 \bar{T}^2}{\bar{\rho}\,|\Delta u|} \frac{\mathcal{A}}{\pi g_v^2}, \qquad (33a)$$

where

$$\mathcal{A} = \int d\omega\, dk\, \frac{k^2}{2} M(\omega, k). \qquad (33b)$$

The quantity $\mathcal{A}$ is the integrated wave action flux upon emission from the convection [see (22) and (23)] with breaking upon emission applied.

Notice that $mB_T(m; z)$ is independent of m as shown in Fig. 5. In analogy with (29) we define f_c as the frac-

tion of the temperature variance that remains as the wave approaches a critical layer. The critical wavenumber m_{critical} is where the temperature variance spectra of (33a) and (25a) intersect:

$$m_{\text{critical}}^2 \approx \bar{\rho}\,|\Delta u|\,N\left(\frac{\pi}{\mathcal{A}}\right). \tag{34a}$$

The breaking factor required for breaking near critical layers is

$$f_c = \frac{m_{\text{critical}}^2}{m_{\text{critical}}^2 + m(z)^2}. \tag{34b}$$

Both m_{critical} and f_c depend on altitude. We constrain f_c to be a monotonically decreasing function of altitude for each mode since we have no mechanism for waves to gain energy as they propagate vertically.

This formulation of wavebreaking gives a prediction for the dependence of the "knee" in the saturated spectrum on altitude. In order to calculate wavebreaking at all heights beneath the zonal wind maximum, we need to determine the value of $\mathcal{A}$ to be used in (34a). We determine this value by calculating the temperature variance spectrum $B_T(m; z)$ at one altitude z and substituting it into (33a). We find that $\mathcal{A}/\pi$ is 4.37 kg s^{-2} for W_c = 1 m s^{-1}, 93.2 kg s^{-2} for W_c = 3 m s^{-1}, and 341 kg s^{-2} for W_c = 5 m s^{-1}. Given $\mathcal{A}$, we can then figure out absolutely what the critical wavenumber m_{critical} is as a function of height.

The effectiveness of this breaking mechanism is demonstrated in Fig. 5. In this figure we show what the temperature variance spectrum at 60 km would be both with and without implementing breaking near critical layers. The critical value of the vertical wavenumber occurs near 0.05 m^{-1}, where wavebreaking creates a knee in the temperature variance spectrum.

For larger forcing amplitudes, the "unbroken" spectrum would become larger, and the knee would move to a smaller vertical wavenumber.

2) Momentum and energy deposition

We compute the accelerations of the mean flow created by convectively generated gravity waves. For this calculation it is necessary to perform the same calculation as was done for Fig. 4 in the first model but with a different background atmosphere. We compute what the acceleration profiles would be if momentum deposition occurred by wavebreaking and by critical layer absorption separately.

Critical layer absorption is like wavebreaking, but simpler. In each layer $(z, z + dz)$ one removes the waves whose zonal phase speed lies in the interval $\bar{u}(z)$, $\bar{u}(z + dz)$, depositing their momentum at the altitude z. With wavebreaking, this momentum would be deposited at a lower level. We shall show that the difference in momentum flux deposition between wavebreaking and critical layer absorption is not large.

In Figs. 6 and 7 we show acceleration profiles for both wavebreaking and critical layer absorption for forcing amplitudes of 3 and 5 m s^{-1}. We have shown the profile resulting from wavebreaking as dashed lines between 55- and 66-km altitude. For W_c = 3 m s^{-1}, the total prograde momentum carried and deposited by the waves is 2.17 × 10^{-2} N m^{-2}, and the total retrograde momentum is 1.02 × 10^{-2} N m^{-2}. The acceleration falls off strongly with altitude because of the c_x^{-3} tail in the momentum flux spectrum. The distribution of the accelerations is strongly skewed toward the bottom of the stable layer, just outside the convection. For W_c = 3 m s^{-1}, the largest prograde acceleration is 2.95 m s^{-1} day^{-1} just above the convection. The acceleration falls off to 10^{-2} m s^{-1} day^{-1} at 67 km. Convectively generated gravity waves provide little acceleration near the zonal wind maximum and, therefore, are not good candidates for sustaining the maximum superrotation.

It is obvious from Figs. 6 and 7 that wavebreaking and critical layer absorption create nearly identical acceleration profiles. The reason for this is that waves break primarily when they are near their critical layers. The difference between the profiles just above the convecting layer arises because the waves that are critically absorbed immediately above the convection have zero phase speed and hence zero momentum flux (see Fig. 4). The waves that break immediately above the convection do carry some momentum.

The wave decelerations at 80 km appear so much larger than accelerations between 55 and 60 km because of the density falloff with height. The integrated retrograde momentum deposition above 67 km is 1.02 × 10^{-2} N m^{-2} for W_c = 3 m s^{-1}. There is less retrograde momentum than prograde momentum because some retrograde waves are reflected downward by a Doppler-created lid. The maximum deceleration from retrograde waves is 86 m s^{-1} day^{-1} for W_c = 3 m s^{-1}. The deceleration is concentrated at 80-km altitude because the zonal wind at that altitude matches the zonal wind where the waves are generated. If we had used a zonal wind profile with a weaker shear above the zonal wind maximum, the eastward waves would have deposited their momentum higher than 80-km altitude.

If there were no wind shear above the maximum zonal wind at 66-km altitude, there would be no critical layers. Then wavebreaking due to the decrease of density would be responsible for the momentum deposition and would occur at high altitude. In Fig. 8, we show the momentum deposition profile that results in an atmosphere without wind shear above 66 km. The zonal wind profile is shown on the right-hand side of the figure. Notice that the units of acceleration have changed from m s^{-1} day^{-1} to m s^{-2}. The prograde acceleration profile just above the convection remains the same as in the previous model, but the retrograde decelerations have moved to much higher altitude and have become much stronger. In essence, the retrograde waves carry

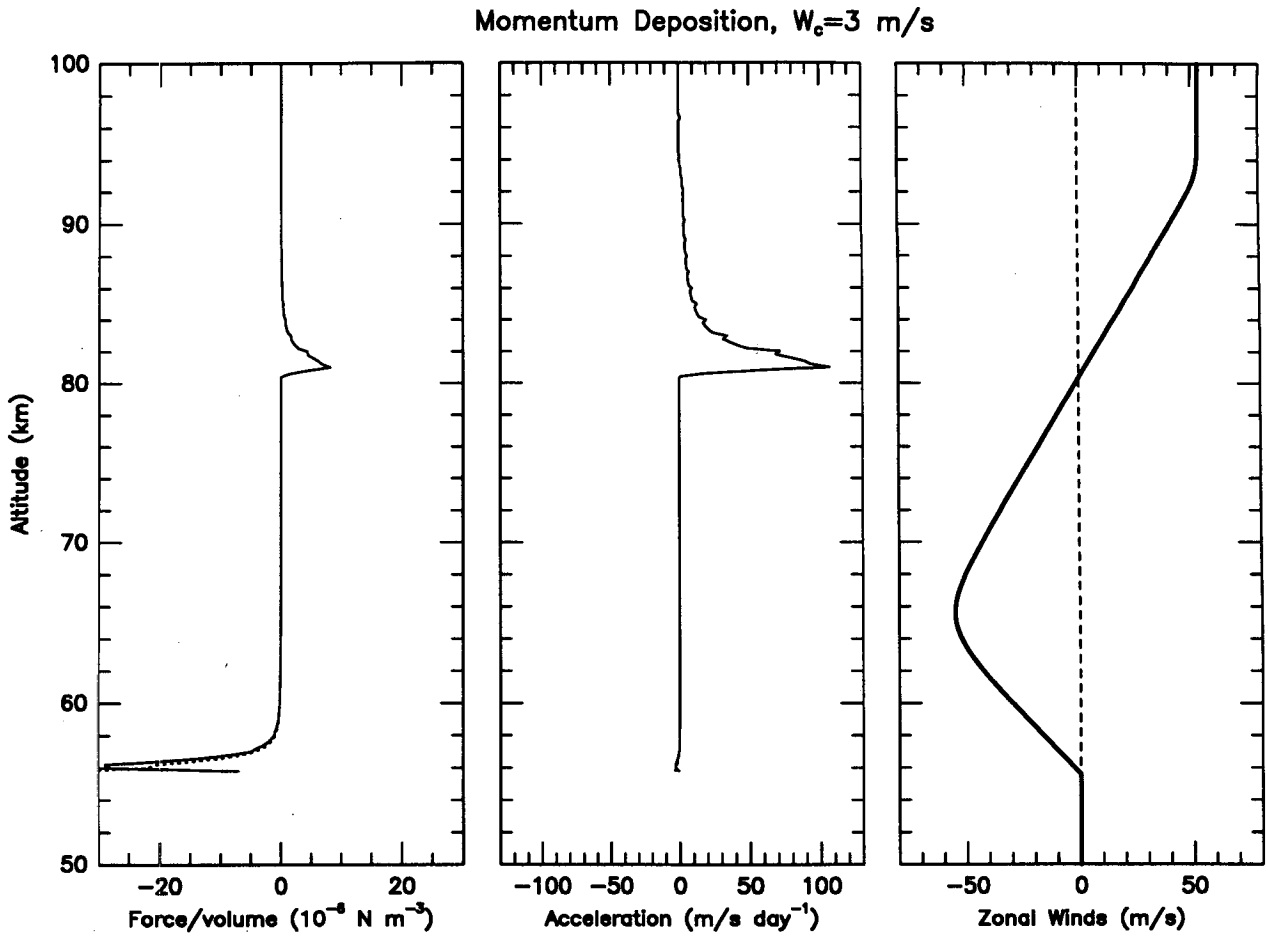

FIG. 6. Momentum deposition profiles for $W_c = 3$ m s^{-1}. We show the momentum deposition rate per unit volume, the momentum deposition rate per unit mass, and the zonal wind profile as functions of altitude for $W_c = 3$ m s^{-1}. The dashed lines refer to deposition by wavebreaking, and the solid lines refer to deposition by critical layer absorption. Barely visible beneath the solid lines, the dashed line is only plotted between 55- and 67-km altitude.

the same amount of retrograde momentum as in the previous model atmosphere, but they do not saturate until they reach much higher altitude. They eventually break where the atmosphere is much less dense; hence, the decelerations are much larger. Had the wave forcing W_c been weaker, the retrograde waves would have broken at a higher altitude. Thus we have demonstrated that the retrograde waves will eventually deposit their momentum and that the wind profile only serves to determine where the retrograde waves will break.

4. Discussion

According to our model, convectively generated gravity waves cannot sustain the winds beyond a few kilometers away from the convection. Waves with phase speeds greater than 3–5 m s^{-1} are not excited in our model. Because of critical layer absorption in this region of strong shear flow, most of these waves are critically absorbed within a few kilometers above the convection. Waves that propagate obliquely to the mean flow can propagate to higher altitudes where they can deposit their momentum. These waves do not carry a substantial amount of momentum, however, since their contribution to the zonal momentum flux falls off as c_x^{-3}. Thus, the zonal wind maximum at 66-km altitude receives little acceleration from these waves.

These conclusions would change if the waves were able to transmit some momentum flux through their critical layers. This might occur because of self-acceleration (Grimshaw 1974; Dunkerton and Fritts 1984) or scattering. If the prograde waves were to deposit all of their westward momentum evenly in the two scale-height region between the top of the convecting layer and the altitude of the zonal wind maximum, the force per unit volume

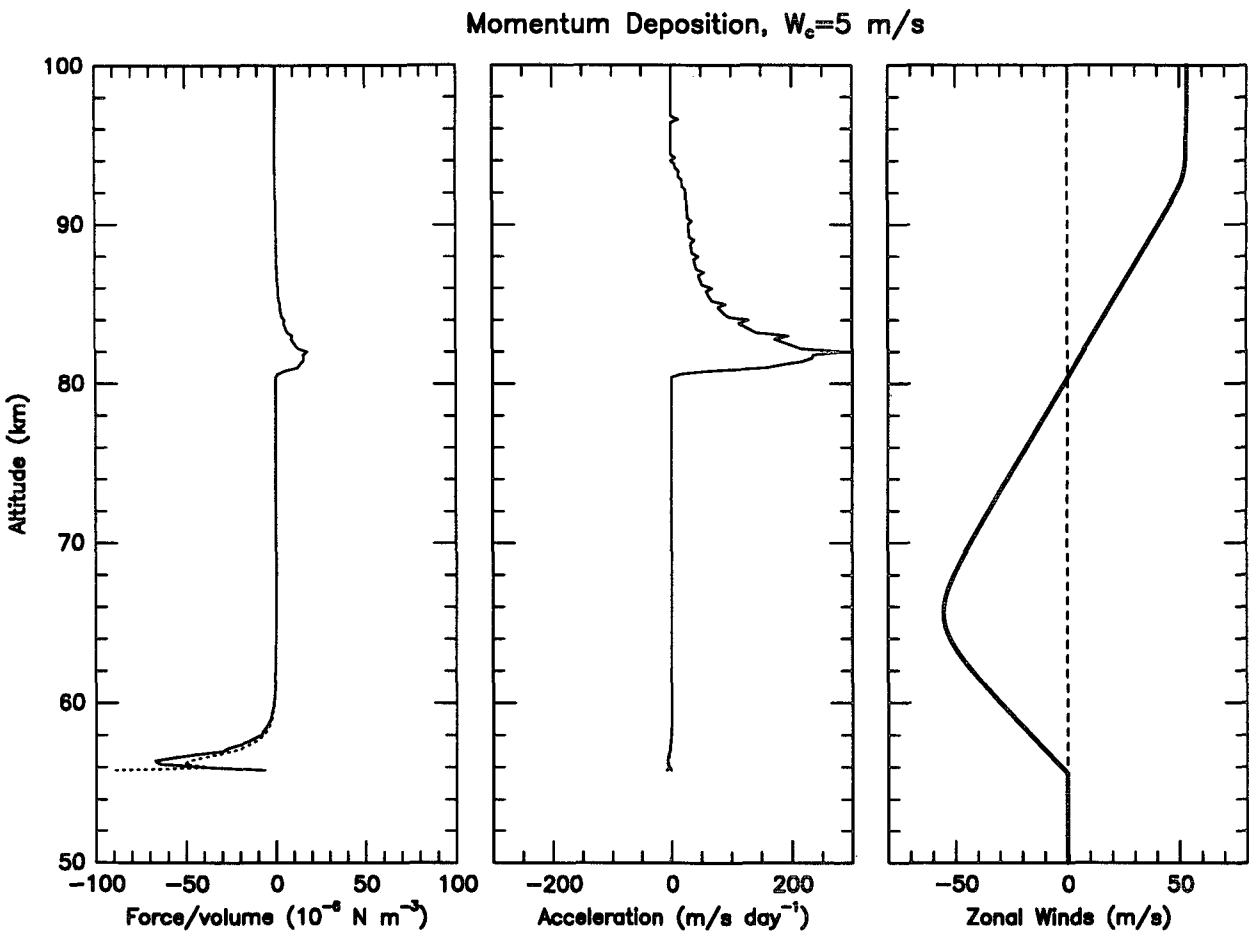

FIG. 7. Momentum deposition profiles for W_c = 5 m s^{-1}. Same as Fig. 6 but for W_c = 5 m s^{-1}.

would be 4.3 × 10^{-5} N m^{-3}. This compares well with Hou and Goody (1985).

Other mechanisms of gravity wave generation pertaining to convection are possible. First, if a zonal wind shear should exist within the convection, the forcing of waves would become more efficient (Sutherland et al. 1994). Second, if the convective eddies impinge on the overlying stable layer, they would present obstacles to the shear flow, which would efficiently generate waves (Clark et al. 1986). Third, should horizontally extended coherent structures exist within the convecting layer, they might generate high horizontal phase-speed waves. If any of these mechanisms are relevant to the convecting layer in the Venus clouds, then the gravity waves excited by the convection might play a more significant role than those that we have investigated.

Convectively generated gravity waves may play a more significant role in supporting the wind shear if the associated wavebreaking were the primary source of drag. In our model, gravity wave momentum is deposited where the gravity waves break. Conceptually, when larger amounts of momentum are deposited, the associated wavebreaking creates stronger dissipative turbulence. This turbulence then exerts a stronger drag on the shear. Thus, even though wave driving falls off rapidly with height in our model, the friction might also drop off rapidly with height, and the zonal wind shear might be in a gravity wave driven steady state. If, however, there are other major sources of friction, such a steady state probably would not exist.

The retrograde (eastward) waves will deposit their momentum above the zonal wind maximum. When the shear is positive above 66 km, the retrograde momentum is deposited where the zonal wind is the same as at the altitude of the convection. In a weaker shear the deposition would take place at higher altitude, and with no shear the deposition is still higher. The amount of retrograde momentum is independent of the wind profile. The waves contribute a large eastward drag above 66 km no matter

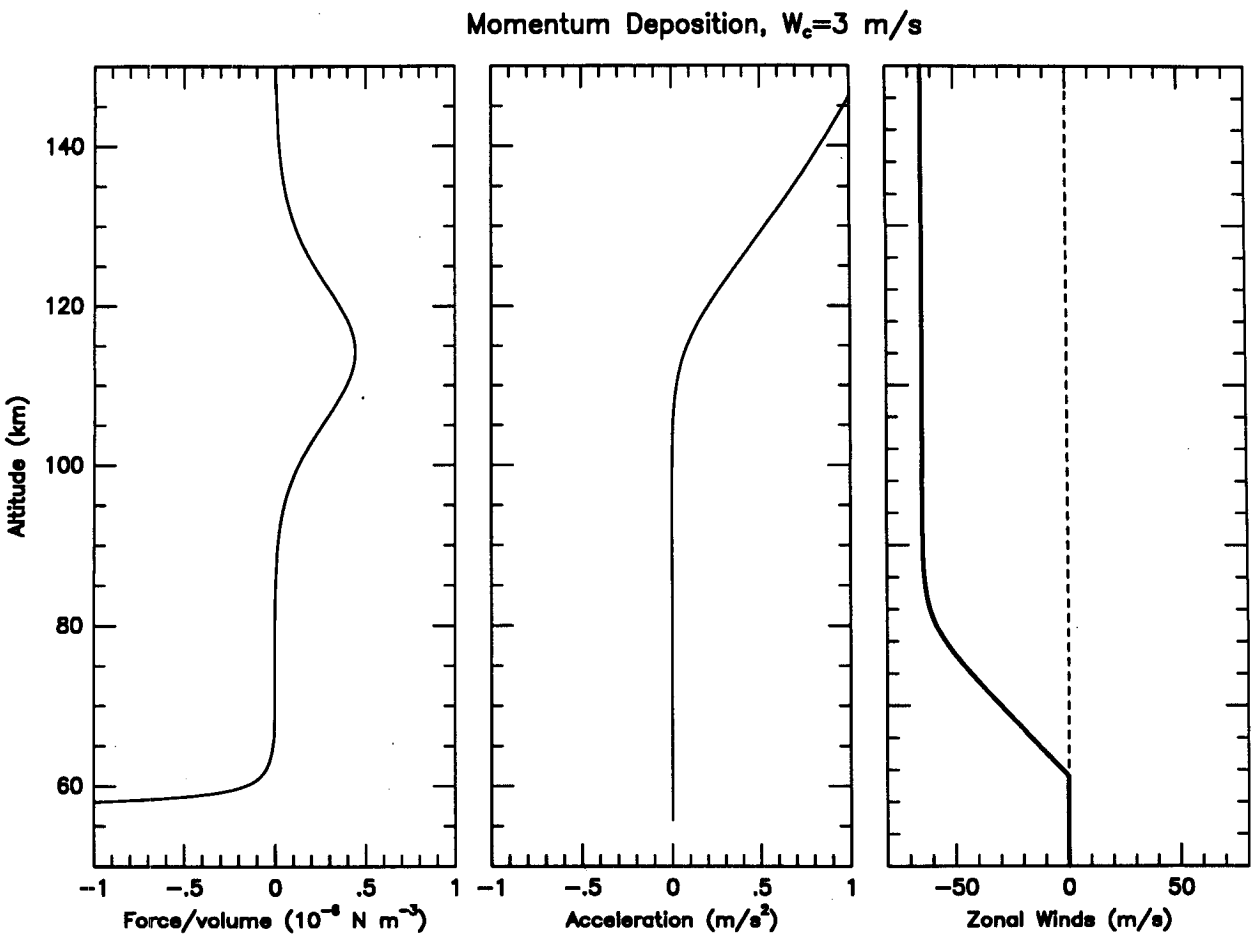

FIG. 8. Momentum deposition profiles in an atmosphere without shear above 66 km. We have used $W_c = 3$ m s^{-1}. Otherwise similar to Figs. 6 and 7 except that the critical layer absorption mechanism is not included.

what the zonal wind profile is. In reality, the mean flow profile should adjust so that this drag is offset by some other westward-forcing high in the Venus atmosphere. Coincidentally, we have found decelerations that are the same order of magnitude as those thought to be exerted by gravity waves in Earth's mesosphere (Leovy 1964; Holton 1982).

In Earth's atmosphere, it is thought that internal gravity waves might help drive the quasi-biennial oscillation (QBO, Holton and Lindzen 1972). It is unlikely that convectively generated gravity waves in Venus's atmosphere could drive a quasi-oscillation such as the QBO because such gravity waves move too slowly. It takes 30–40 m s^{-1} phase speeds in Earth's atmosphere to drive a QBO with an amplitude of 30 m s^{-1}, but the gravity waves we have described in Venus's atmosphere move at about 5 m s^{-1}, and the wind maximum is nearly 60 m s^{-1} faster than the source region.

Acknowledgments. We wish to thank Peter Goldreich for much assistance in this work. It was supported by a National Science Foundation Graduate Fellowship and by NAGW-1956 of the NASA Planetary Atmospheres program.

APPENDIX A

The Function $h(z)$

Because waves encounter regions where they can propagate and regions where they cannot propagate, we must determine how to connect these different types of wave behavior. Connecting regions of propagation to regions of nonpropagation requires *connection formulas.* For regions of propagation, the square of the vertical wavenumber is greater than zero and

$$h(z) \approx \tilde{\omega}\sqrt{\frac{q|m|}{\bar{\rho}}}\,(c_1 e^{iq} + c_2 e^{-iq}).$$

For regions of nonpropagation, the square of the vertical wavenumber is less than zero and

$$h(z) \approx \tilde{\omega}\sqrt{\frac{q|m|}{\bar{\rho}}}\,(c_3 e^{q} + c_4 e^{-q}).$$

We note that the dispersion relation m^2 and the phase q are defined by (9) and (11).

We find the relationship between the sets of coefficients (c_1, c_2) and (c_3, c_4) by modeling the behavior of the solution between regions of propagation and regions of nonpropagation. We do this in much the same manner as has been done for the Schroedinger equation. The major difference between finding connection formulas for the Schroedinger equation and those for gravity waves is that the zero of the vertical wavenumber occurs in the numerator of the undifferentiated term for the Schroedinger equation versus in the denominator of the differentiated term for gravity waves. This difference leads to slightly different solutions.

In finding the connection formulas, we assume that m^2 is continuous, approximate $m^2 = a^3 z$ and account for the $\tilde{\omega}$ and $\bar{\rho}$ dependence with a factor $\tilde{\omega}/(\bar{\rho})^{1/2}$. The remaining equation is

$$\frac{\partial}{\partial z}\left[\frac{1}{m^2}\frac{\partial}{\partial z}\left(\frac{\sqrt{\bar{\rho}}}{\tilde{\omega}}h\right)\right] + \frac{\sqrt{\bar{\rho}}}{\tilde{\omega}}h = 0.$$

The solution to this equation is

$$\frac{\sqrt{\bar{\rho}}}{\tilde{\omega}}h(z) = \left(\frac{2}{3}a^3\right)^{1/2} \times z \begin{cases} AJ_{2/3}\left[\frac{2}{3}(az)^{3/2}\right] + BJ_{-2/3}\left[\frac{2}{3}(az)^{3/2}\right] \\ \quad \text{for} \quad z > 0, \quad m^2 > 0 \\ AI_{2/3}\left(\frac{2}{3}|az|^{3/2}\right) + BI_{-2/3}\left(\frac{2}{3}|az|^{3/2}\right) \\ \quad \text{for} \quad z < 0, \quad m^2 < 0. \end{cases} \tag{A1}$$

The functions $J_{2/3}$ and $J_{-2/3}$ are Bessel functions of the 2/3 order. The functions $I_{2/3}$ and $I_{-2/3}$ are modified Bessel functions of the 2/3 order. The coefficients A, B are general. The phase q is defined from $z = 0$ so that $q = (2/3)|az|^{3/2}$.

We wish to find out how (A1) relates to the usual WKBJ solutions. To do so, we examine the asymptotic expansions of the Bessel functions [asymptotic expansions to these Bessel functions can be found in Abramowitz and Stegun (1972, pp. 365 and 377–378)]. We require a solution proportional to $(m)^{1/2}$ in the far field and substitute $m^2 = a^3 z$. For $m^2 > 0$ we find that

$$h(z) = \tilde{\omega}\sqrt{\frac{m}{\bar{\rho}}}\left[A\cos\left(q - \frac{7\pi}{12}\right) + B\cos\left(q + \frac{\pi}{12}\right)\right] \tag{A2}$$

in the asymptotic expansion. Therefore, for some substantial value of the phase q from a turning point, the connection formulas accurately reproduce the general WKBJ solutions. With some algebra, one can find the relationship between A, B and c_1, c_2 [see (10)].

In comparing the solution for $m^2 < 0$ to the solution in the WKBJ approximation, we notice that even though the asymptotic form for both $I_{2/3}(q)$ and $I_{-2/3}(q)$ is a growing exponential, the asymptotic form for $I_{2/3}(q) - I_{-2/3}(q)$ is a decaying exponential. For this reason we find the asymptotic form of the general solution for $m^2 < 0$ to be

$$h(z) = \tilde{\omega}\sqrt{\frac{|m|}{2\pi\bar{\rho}}}\left[(A + B)e^{q} - \frac{\sqrt{3}}{2}(A - B)e^{-q}\right]. \tag{A3}$$

Like the solution for $m^2 > 0$, the asymptotic form of the connection formula for $m^2 < 0$ matches the WKBJ approximate solution in character for sufficiently large q. This enables us to relate A, B and c_3, c_4 [see (12)].

APPENDIX B

The derivative of $h(z)$

In this appendix we investigate the derivative of the homogeneous solution to $\mathcal{L}h = 0$. It was mentioned in the text that simply taking a finite difference of $h(z)$ is incorrect because it would introduce third-order terms. We instead wish to find a correct second-order WKBJ solution for $\partial h/\partial z$.

We start by taking the derivative of $\mathcal{L}h$ with respect to z after multiplying it by $\tilde{\omega}^2/\bar{\rho}$. After defining $\eta \equiv \bar{\rho}/(N^2 - \tilde{\omega}^2)\partial h/\partial z$, we get

$$\frac{\partial}{\partial z}\left(\frac{\tilde{\omega}^2}{\bar{\rho}}\frac{\partial \eta}{\partial z}\right) + \frac{(N^2 - \tilde{\omega}^2)k^2}{\bar{\rho}}\eta = 0.$$

The solution for h is given in appendix A by (A1). The asymptotic expansion of this solution gave exactly the general WKBJ solutions [(A2) and (A3)]. In the same spirit we find the connection formulas for η, and in solving for $\partial h/\partial z$ we get

$$\frac{\partial h}{\partial z} = \tilde{\omega}\sqrt{\frac{q|m|}{\bar{\rho}}} \begin{cases} CJ_{1/3}(q) + DJ_{-1/3}(q) \\ \quad \text{for} \quad m^2 > 0, \quad \text{and} \\ CI_{1/3}(q) + DI_{-1/3}(q) \\ \quad \text{for } m^2 < 0. \end{cases} \tag{B1}$$

This is the correct second-order WKBJ solution for the derivative of $h(z)$ with respect to height.

Near a turning point, an explicit derivative of (A1) agrees with the derivative in (B1) above provided that the coefficient $\tilde{\omega}/(\bar{\rho})^{1/2}$ is held constant. This can be shown by setting $m^2 = a^3 z$ [hence $q = (2/3)|az|^{3/2}$] and taking a derivative of h in z while holding $\tilde{\omega}/(\bar{\rho})^{1/2}$ constant. The derivatives of $J_{1/3}$ and $J_{-1/3}$ are found in Abramowitz and Stegun (1972). The coefficients C and D are related to A and B by

$$C = -|m|B$$
$$D = |m|A. \qquad \text{(B2)}$$

Thus, finite differencing $h(z)$ near a turning point gives the correct second-order quantity provided that the coefficient $\tilde{\omega}/(\bar{\rho})^{1/2}$ is held constant.

Far from a turning point, an explicit derivative of (A2) agrees with the derivative in (B1) provided that the coefficient $\tilde{\omega}(m/\bar{\rho})^{1/2}$ is held constant. This can be shown by simply taking a derivative of h, given by expression (A2), in z while holding the coefficient $\tilde{\omega}(m/\bar{\rho})^{1/2}$ constant. Using the relations given in (B2), this derivative matches the derivative in (B1). Thus, finite differencing $h(z)$ far from a turning point gives the correct second-order quantity provided that the coefficient $\tilde{\omega}(m/\bar{\rho})^{1/2}$ is held constant.

In conclusion, the derivative of the function $h(z)$ is found numerically by finite differencing $h(z)$ holding the leading factor of $\tilde{\omega}/\sqrt{\bar{\rho}}$ constant:

$$\frac{\partial h}{\partial z} = \frac{\tilde{\omega}}{(\bar{\rho})^{1/2}} \frac{\partial}{\partial z}\left[\frac{\sqrt{\bar{\rho}}}{\tilde{\omega}} h(z)\right].$$

Even though this is not what is explicitly required for calculating $\partial h/\partial z$ far from a turning point, it is permissible by the WKBJ condition. Since this condition holds that variations in the vertical wavenumber m are small over a distance $2\pi/m$, holding m constant is valid when taking a derivative far from a turning point.

REFERENCES

Abramowitz, J., and I. A. Stegun, 1972: *Handbook of Mathematical Functions.* Dover Publications, 1046 pp.

Andrews, D. G., and M. E. McIntyre, 1976: Planetary waves in horizontal and vertical shear: The generalized Eliassen–Palm relation and the mean zonal acceleration. *J. Atmos. Sci.*, **33,** 2031–2048.

——, J. R. Holton, and C. B. Leovy, 1987: *Middle Atmosphere Dynamics.* Academic Press, 489 pp.

Belton, M. J. S., G. R. Smith, G. S. Schubert, and A. D. DelGenio, 1976: Cloud patterns, waves and convection in the Venus atmosphere. *J. Atmos. Sci.*, **33,** 1394–1417.

Booker, J. R., and F. P. Bretherton, 1967: The critical layer for internal gravity waves in a shear flow. *J. Fluid. Mech.*, **27,** 513–539.

Bretherton, F. P., 1966: The propagation of groups of internal gravity waves in a shear flow. *Quart. J. Roy. Meteor. Soc.*, **92,** 466–480.

Clark, T. L., T. Hauf, and J. P. Kuettner, 1986: Convectively forced internal gravity waves: Results from two-dimensional numerical experiments. *Quart. J. Roy. Meteor. Soc.*, **112,** 899–925.

Crisp, D., 1989: Radiative forcing of the Venus mesosphere. Part II: Thermal fluxes, cooling rates, and radiative equilibrium temperature. *Icarus,* **77,** 391–413.

Dewan, E. M., and R. E. Good, 1986: Saturation and the "universal" spectrum for vertical profiles of horizontal scalar winds in the atmosphere. *J. Geophys. Res.*, **91,** 2742–2748.

Dunkerton, T. J., and D. C. Fritts, 1984: Transient gravity wave–critical layer interaction. Part I: Convective adjustment and the mean zonal acceleration. *J. Atmos. Sci.*, **41,** 992–1007.

Fovell, R., D. Durran, and J. R. Holton, 1992: Numerical simulations of convectively generated stratospheric gravity waves. *J. Atmos. Sci.*, **49,** 1427–1442.

Geller, M. A., H. Tanaka, and D. C. Fritts, 1975: Production of turbulence in the vicinity of critical levels for internal gravity waves. *J. Atmos. Sci.*, **32,** 2125–2135.

Gierasch, P. J., 1975: Meridional circulation and the maintenance of the Venus atmospheric rotation. *J. Atmos. Sci.*, **32,** 1038–1044.

Goldreich, P., and P. Kumar, 1990: Wave generation by turbulent convection. *Astrophys. J.*, **363,** 694–704.

Grimshaw, R., 1974: Internal gravity waves in a slowly varying dissipative medium. *Geophys. Fluid Dyn.*, **6,** 131–148.

Hide, R., 1969: Dynamics of the atmospheres of the major planets. *J. Atmos. Sci.*, **26,** 841–847.

——, 1970: Equatorial jets in planetary atmospheres. *Nature,* **225,** 254–255.

Hines, C. O., 1991: The saturation of gravity waves in the middle atmosphere. Part I: Critique of linear-instability theory. *J. Atmos. Sci.*, **48,** 1348–1359.

Hodges, R. R., Jr., 1967: Generation of turbulence in the upper atmosphere by internal gravity waves. *J. Geophys. Res.*, **72,** 3455–3458.

Holton, J. R., 1982: The role of gravity wave induced drag and diffusion in the momentum budget of the mesosphere. *J. Atmos. Sci.*, **39,** 791–799.

——, and R. S. Lindzen, 1972: An updated theory for the quasi-biennial cycle of the tropical stratosphere. *J. Atmos. Sci.*, **29,** 1076–1080.

Hou, A. Y., and R. M. Goody, 1985: Diagnostic requirements for the superrotation on Venus. *J. Atmos. Sci.*, **42,** 413–432.

——, and B. F. Farrell, 1987: Superrotation induced by critical-level absorption of gravity waves on Venus: An assessment. *J. Atmos. Sci.*, **44,** 1049–1061.

Ingersoll, A. P., D. Crisp, A. W. Grossman, and the VEGA balloon science team, 1987: Estimates of convective heat fluxes and gravity wave amplitudes in the Venus middle cloud layer from VEGA balloon measurements. *Adv. Space Res.*, **7**(12), 343–349.

Ishimaru, A., 1978: *Wave Propagation and Scattering in Random Media. Vol. 1, Single scattering and Transport Theory,* Academic Press, 250 pp.

Landau, L. D., and E. M. Lifshitz, 1987: *Fluid Mechanics.* 2d ed. Pergamon Press, 539 pp.

Leovy, C. B., 1964: Simple models of thermally driven mesospheric circulation. *J. Atmos. Sci.*, **21,** 327–341.

Lighthill, M. J., 1952: On sound generated aerodynamically. Part I: General theory. *Proc. Roy. Soc. London, Ser. A,* **211,** 564–587.

Lindzen, R. S., and J. Forbes, 1983: Turbulence originating from convectively stable internal waves. *J. Geophys. Res.*, **88,** 6549–6553.

Lumley, J. L., and H. A. Panofsky, 1964: *The Structure of Atmospheric Turbulence.* John Wiley & Sons, 239 pp.

Morse, P. M., and H. Feshbach, 1953: *Methods of Theoretical Physics.* Vol. 1. McGraw-Hill.

Ogura, Y., and N. A. Phillips, 1962: Scale analysis of deep and shallow convection in the atmosphere. *J. Atmos. Sci.*, **19,** 173–179.

Sagdeev, R. Z., V. M. Linkin, J. E. Blamont, and R. A. Preston, 1986a: The VEGA Venus balloon experiment. *Science,* **231,** 1407–1408.

——, and Coauthors, 1986b: Overview of VEGA Venus balloon in situ meteorological measurements. *Science,* **231,** 1411–1414.

Schubert, G., 1983: General circulation and the dynamical state of the Venus atmosphere. *Venus,* D. M. Hunten, L. Colin, T. M. Donahue, and V. I. Moroz, Eds., University of Arizona Press, 681–765.

——, and R. L. Walterscheid, 1984: Propagation of small-scale acoustic–gravity waves in the Venus atmosphere. *J. Atmos. Sci.,* **41,** 1202–1213.

Schwarzschild, M., 1958: *Structure and Evolution of the Stars.* Princeton University Press, 296 pp.

Seiff, A., D. B. Kirk, R. E. Young, R. C. Blanchard, J. T. Findlay, G. M. Kelly, and S. C. Sommer, 1980: Measurements of thermal structure and thermal contrasts in the atmosphere of Venus and related dynamical observations: Results from the four Pioneer Venus probes. *J. Geophys. Res.,* **85,** 7903–7933.

Smith, S. A., D. C. Fritts, and T. E. VanZandt, 1987: Evidence for a saturated spectrum of atmospheric gravity waves. *J. Atmos. Sci.,* **44,** 1404–1410.

Stein, R. F., 1967: Generation of acoustic and gravity waves by turbulence in an isothermal stratified atmosphere. *Solar Phys.,* **2,** 385–432.

Sutherland, B. R., C. P. Caulfield, and W. R. Peltier, 1994: Internal gravity wave generation and hydronamic instability. *J. Atmos. Sci.,* **51,** 3261–3280.

Woo, R., and J. W. Armstrong, 1980: Radio occultation measurements of turbulence in the Venus atmosphere by Pioneer Venus. *J. Geophys. Res.,* **85,** 8031–8038.

Young, R. E., and J. B. Pollack, 1977: A three-dimensional model of dynamical processes in the Venus atmosphere. *J. Atmos. Sci.,* **34,** 1315–1351.